

Modular Commutators in Conformal Field Theory

Yijian Zou,^{1,*} Bowen Shi,^{2,*} Jonathan Sorce,¹ Ian T. Lim,³ and Isaac H. Kim⁴

¹Stanford Institute for Theoretical Physics, Stanford University, Palo Alto, CA 94305, USA

²Department of Physics, University of California at San Diego, La Jolla, CA 92093, USA

³Department of Physics and Astronomy, University of California, Davis, CA 95616, USA

⁴Department of Computer Science, University of California, Davis, CA 95616, USA

(Dated: June 6, 2022)

The modular commutator is a recently discovered multipartite entanglement measure that quantifies the chirality of the underlying many-body quantum state. In this Letter, we derive a universal expression for the modular commutator in conformal field theories in 1+1 dimensions and discuss its salient features. We show that the modular commutator depends only on the chiral central charge and the conformal cross ratio. We test this formula for a gapped 2+1-dimensional system with a chiral edge, i.e., the quantum Hall state, and observe excellent agreement with numerical simulations. Furthermore, we propose the geometric dual of the modular commutator in the AdS/CFT correspondence. We argue that the modular commutator can be obtained from a set of crossing angles between intersecting Ryu-Takayanagi surfaces.

One of the major overarching themes of research in theoretical physics over the past few decades has been the study of entanglement in interacting quantum many-body systems. Calculation of the canonical measure of entanglement — entanglement entropy — has played a crucial role in elucidating the physics of topological order [1, 2], conformal field theory [3], and holographic duality [4].

Recently, an entirely new entanglement measure known as the *modular commutator* was introduced [5, 6]. The modular commutator is defined as $J(A, B, C)_\rho := i\text{Tr}(\rho_{ABC}[\ln \rho_{AB}, \ln \rho_{BC}])$ for a tripartite quantum state ρ_{ABC} , and unlike other known entanglement measures, it is odd under time reversal. In the context of topologically ordered systems in 2+1D, the modular commutator was used to extract the chiral central charge of the edge theory [5, 6].

In this Letter, we derive a universal expression for the modular commutator in conformal field theories in 1+1D and discuss its physical implications. Let A, B , and C be three contiguous spacetime intervals; see Fig. 1(a). In this setup, we derive a general expression for $J(A, B, C)$. If the subsystems lie in a single-time slice, the expression simplifies to the following:

$$J(A, B, C)|_\Omega = \frac{\pi c_-}{6}(2\eta - 1), \quad (1)$$

where $\eta = \frac{(x_2 - x_1)(x_4 - x_3)}{(x_3 - x_1)(x_4 - x_2)}$ is the cross ratio and $c_- = c_L - c_R$ is the chiral central charge of the 1+1D CFT, and $|\Omega\rangle$ is the vacuum state. Using the standard conformal mapping of the complex plane to an infinite cylinder, expressions for the modular commutator for finite systems and infinite systems at finite temperature are also derived.

We primarily discuss two applications. First, we argue that Eq. (1) can be a useful tool to study the entanglement structure of 2+1D chiral gapped systems at their edges. Specifically, consider three contiguous intervals

A, B , and C at the edge of a disk; see Fig. 3(a). We propose the following formula — based on an argument utilizing Eq. (1) — for the modular commutator:

$$J(A, B, C)|_{\psi_{2D}} = \frac{\pi c_-}{3}\eta, \quad (2)$$

where c_- is the chiral central charge of the 2+1D system (defined as a coefficient appearing in the edge energy current [7–9]) and $|\psi_{2D}\rangle$ is the ground state. We test Eq. (2) numerically for the Chern insulator and $p+ip$ topological superconductor, demonstrating excellent agreement.

When A, B and C cover the entire edge (see Fig. 3(b)), i.e., $\eta = 1$, we provide an independent information-theoretic argument for a stronger result:

$$J(A, B, C)|_{\tilde{\psi}_{2D}} = \frac{\pi}{3}c_-, \quad (3)$$

where $|\tilde{\psi}_{2D}\rangle$ is any state which is indistinguishable from $|\psi_{2D}\rangle$ in the bulk region. We emphasize the generality of Eq. (3) in two directions. This equation holds even if there is an excitation localized at the edge. Moreover, the argument continues to hold even if the edge is deformed continuously. The underlying argument — based on the properties of modular commutator [5, 6] and the techniques from entanglement bootstrap [10] — reveals that the robustness of this result originates from the entanglement area law of the bulk.

Second, we propose a holographic interpretation of Eq. (1). Our interpretation rests on an observation that Eq. (1) can be recast as

$$J(A, B, C)|_\Omega = \frac{\pi c_-}{6} \cos \theta, \quad (4)$$

where θ is the crossing angle of the two geodesics (i.e., two Ryu-Takayanagi surfaces [4]) in AdS₃, each anchored at the boundaries of AB and BC , respectively. We verify this correspondence at both zero and finite temperature and propose a generalization.

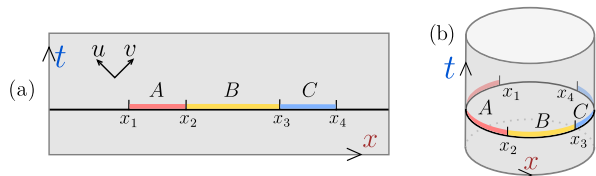


FIG. 1. (a) Three contiguous intervals A, B , and C , on a single-time slice. (b) Contiguous intervals on a circle S^1 with circumference L .

Our approach to derive Eq. (1) will be geometric in nature. The main advantage of this derivation is that it makes the generalization of Eq. (1) to spacetime intervals straightforward. Alternative derivations shall be discussed in the Supplementary Material (SM) as well.

Geometric derivation— Our derivation of Eq. (1) is based on the following two observations. First, the modular commutator $J(A, B, C)$ can be viewed as the response of the entanglement entropy under the modular flow [6]. Second, for a 1+1D CFT, the modular flow for a finite interval generates a special conformal transformation that keeps the two ends of the interval fixed [11–13]. Thus, we will compute the modular commutator $J(A, B, C)$ by the change of the entropy S_{BC} from the infinitesimal conformal transformation generated by the modular flow.

The *modular flow* of an operator O with respect to a subsystem A is defined as $O(s) := \rho_A^{is} O \rho_A^{-is}$ for some $s \in \mathbb{R}$. We consider the action of the modular flow associated with the interval AB . Define the following one-parameter family of density matrices: $\rho_{ABC}(s) := \rho_{AB}^{is} \rho_{ABC} \rho_{AB}^{-is}$. The response of the von Neumann entropy of $\rho_{BC}(s) = \text{Tr}_A(\rho_{ABC}(s))$ under this flow is related to the modular commutator by [6]:

$$\left. \frac{dS(\rho_{BC}(s))}{ds} \right|_{s=0} = -J(A, B, C)_\rho, \quad (5)$$

where $S(\rho) := -\text{Tr}(\rho \ln \rho)$ is the entanglement entropy.

In the Lorentzian spacetime, the reduced density matrix of the interval AB completely determines observables inside the *causal diamond*, the domain of dependence of AB . For a CFT, the modular flow can be achieved by a conformal transformation restricted to the interior of the causal diamond. The relevant vector fields are illustrated in Fig. 2.

Now we can use the following regulated form of the single-interval entanglement entropy for chiral CFTs in 1+1D [14]:

$$S_{BC} = \frac{c_L}{12} \ln \frac{(v_4 - v_2)^2}{\epsilon_{v2}\epsilon_{v4}} + \frac{c_R}{12} \ln \frac{(u_4 - u_2)^2}{\epsilon_{u2}\epsilon_{u4}}, \quad (6)$$

where $u = t - x$ and $v = x + t$ are light-cone coordinates, and $\epsilon_{u(v)2(4)}$ denotes the UV cutoffs in the u and v directions at the endpoints x_2 and x_4 .

Note that the point x_4 is unaffected by the modular flow with respect to AB , because it is outside the causal

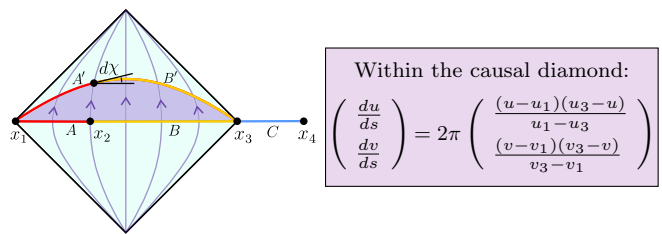


FIG. 2. Modular flow in the interior of the causal diamond (domain of dependence of AB) and the associated vector field. Under an infinitesimal flow by a parameter ds , interval AB becomes $A'B'$ and a boost angle $d\chi$ develops at the left end of B' .

diamond. Thus, u_4, v_4 and $\epsilon_{u4}, \epsilon_{v4}$ remain unchanged; the change only occurs at x_2 . Importantly, the cutoffs $\epsilon_{u(v)2(4)}$ transform as null vectors. Thus, they are rescaled by the local boost angle (see Fig. 2),

$$d \ln \epsilon_{v2} = -d \ln \epsilon_{u2} = d\chi, \quad (7)$$

where $d\chi = \frac{2\pi(x_{23}-x_{12})}{x_{13}} ds$ is the boost angle at x_2 . Here we use the convention $x_{ij} = x_j - x_i$. Differentiating Eq. (6) and using Eq. (7) we obtain

$$J(A, B, C)_{|\Omega} = \frac{\pi c_-}{6} (2\eta - 1), \quad (8)$$

where $c_- = c_L - c_R$ and the cross ratio $\eta = \frac{x_{12}x_{34}}{x_{13}x_{24}}$. Generalization of Eq. (8) to general Cauchy surfaces is straightforward; see the SM for details.

Our expression for $J(A, B, C)_{|\Omega}$ possesses a set of important properties, summarized below. Firstly, J is odd under time reversal, which exchanges c_L and c_R . This is in contrast with other entanglement measures such as the entanglement entropy, which are even under time reversal. Secondly, J is odd under the map $\eta \rightarrow 1 - \eta$. In particular, $J = 0$ at $\eta = 1/2$ where the modular commutator changes sign. Thirdly, as the length of one interval gets small, J does not vanish but takes on universal values. As $x_1 \rightarrow x_2$ or $x_3 \rightarrow x_4$, $\eta \rightarrow 0$ and $J \rightarrow -\pi c_-/6$, and similarly, as $x_2 \rightarrow x_3$, $\eta \rightarrow 1$ and $J \rightarrow \pi c_-/6$. In fact, we shall later see that the universal difference $J(\eta = 1) - J(\eta = 0) = \pi c_-/3$ is exactly the modular commutator for 2D chiral topological order. Lastly, if $c_- \neq 0$, we have $J = \pi c_-/6 \neq 0$ when ABC is the entire circle. This distinguishes $|\Omega\rangle$ from any pure state on a Hilbert space factorized into a tensor product on spatial regions, as the latter necessarily has $J = 0$. Thus, $c_- \neq 0$ is incompatible with any lattice regularization (see also [15] for an alternative argument).

More generally, one can consider a thermal state at inverse temperature β on a circle of circumference L , denoted as $\rho^{(\beta; L)}$. Through a conformal mapping from the complex plane to the cylinder [16], one can show that the modular commutator $J(A, B, C)$ remains to be in the

form in Eq. (1) in two limits, $\beta/L \rightarrow \infty$ or $L/\beta \rightarrow \infty$, with the cross ratio η replaced by $\eta_{\text{eff}}^{(\beta;L)}$:

$$\eta_{\text{eff}}^{(\beta;L)} = \begin{cases} \frac{\sin(\pi x_{12}/L) \sin(\pi x_{34}/L)}{\sin(\pi x_{13}/L) \sin(\pi x_{24}/L)}, & \beta/L \rightarrow \infty, \\ \frac{\sinh(\pi x_{12}/\beta) \sinh(\pi x_{34}/\beta)}{\sinh(\pi x_{13}/\beta) \sinh(\pi x_{24}/\beta)}, & L/\beta \rightarrow \infty. \end{cases} \quad (9)$$

Otherwise the value η_{eff} may depend on the operator content of the CFT; the exact form is currently unknown.

Chiral thermal state— The modular commutator can be nonzero even for non-chiral CFTs, provided that the temperatures for the left- and the right-moving modes are unequal. We refer to such states as *chiral thermal states* [17–19]:

$$\rho^{(\beta_L, \beta_R; L)} = \frac{1}{Z} e^{-\beta_L H_L - \beta_R H_R}. \quad (10)$$

Here H_L and H_R are the Hamiltonians of the left- and right-moving sectors, respectively. Similarly, (β_L, β_R) represent inverse temperatures for the respective modes.

There are a few reasons to study chiral thermal states. First, a chiral thermal state can be obtained by applying the Lorentzian boost to the thermal state. Second, there are concrete lattice models whose underlying state at low temperature can be well-described by a chiral thermal state. For instance, it was noted that the reduced density matrix near the edge of a chiral topological order in 2 + 1D can be represented by a chiral thermal state with $(\beta_L, \beta_R) = (\infty, \text{finite})$ [18]. Third, as we show in the SM, one can sometimes explicitly construct chiral thermal states in some lattice model, making the numerical verification tractable.

From Eq. (9), for a general chiral thermal state $\rho^{(\beta_L, \beta_R; L)}$ we have

$$J(A, B, C)_{\rho^{(\beta_L, \beta_R; L)}} = \frac{\pi}{3} c (\eta_{\text{eff}}^{(\beta_L; L)} - \eta_{\text{eff}}^{(\beta_R; L)}), \quad (11)$$

where $c = c_R = c_L$. We test Eq. (11) for the lattice chiral thermal states and find excellent agreement (see SM for details).

Edge of 2+1D chiral topological order — The chiral thermal state can provide insights into the edge of 2+1D gapped systems with a non-zero chiral central charge, denoted as \mathfrak{c}_- [7–9, 18]. (We choose a different font to distinguish two concepts: the chiral central charge \mathfrak{c}_- of a 2+1D gapped phase versus c_- for a 1+1D chiral CFT.)

Consider a ground state $|\psi_{2D}\rangle$ on a disk for concreteness; see Fig. 3. For an annulus which covers the entire edge, e.g., the annulus in Fig. 3(a), the reduced density matrix of $|\psi_{2D}\rangle$, can be viewed as a 1+1D system. If the edge is completely chiral, (that is when, e.g., it only has left-moving modes but not right-moving modes,) it is expected to be described by a chiral thermal state whose c equals to \mathfrak{c}_- [18].

Then by applying Eq. (11) to the interval choice in Fig. 3(a) and taking $\beta_L = \infty$, $\beta_R \ll L_A, L_B, L_C$ (the

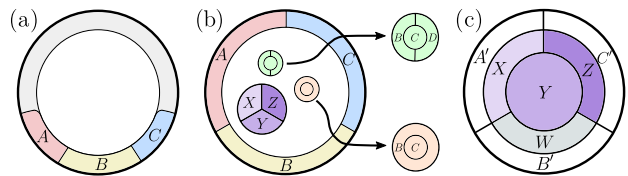


FIG. 3. A 2+1D gapped chiral system on a disk and various choices of subsystems. The sizes (width) for subsystems within the bulk (adjacent to the edge) are large compared to the bulk correlation length.

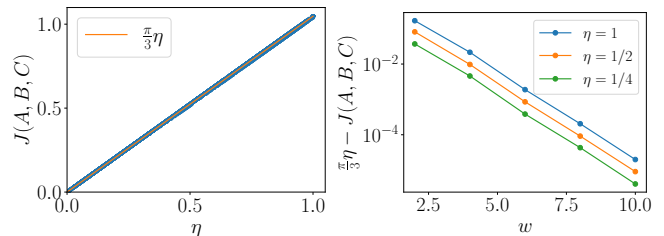


FIG. 4. $J(A, B, C)$ versus η for the Chern insulator, which is realized by filling the lowest band of the Hofstadter model with flux $\pi/2$. We use a square lattice on a cylinder with circumference 144 and height 32. A, B, C are rectangular strips on the boundary with length L_A, L_B, L_C and width w . Left: We fix $w = 10$ and vary the lengths L_A, L_B, L_C . Right: We choose several (L_A, L_B, L_C) and vary w . The three choices $(L_A, L_B, L_C) = (48, 48, 48), (36, 36, 36), (24, 48, 24)$ correspond to $\eta = 1, 1/2, 1/4$, respectively.

lengths of the regions), we arrive at a prediction

$$J(A, B, C)_{|\psi_{2D}\rangle} = \frac{\pi}{3} \mathfrak{c}_- \eta \quad (12)$$

We tested this formula numerically for a Chern insulator and observed excellent agreement; see Fig. 4. We propose this formula to hold for general translation invariant topologically ordered systems in 2+1D.

Topological argument— An interesting observation is that Eq. (12) becomes $J = \frac{\pi}{3} \mathfrak{c}_-$ when the union of intervals A, B , and C is the entire annulus, as shown in Fig. 3(b). In other words, when $\eta = 1$, the modular commutator becomes topological. Here we present an entirely different argument for this formula, based on the entanglement area law of the 2+1D bulk [1, 2]. Our argument reveals an extra degree of robustness of this expression:

$$J(A, B, C)_{|\tilde{\psi}_{2D}\rangle} = \frac{\pi}{3} \mathfrak{c}_- \quad \text{for Fig. 3(b)}. \quad (13)$$

We show that Eq. (13) holds for any state $|\tilde{\psi}_{2D}\rangle$ locally indistinguishable from the ground state within the bulk. Note that we need not assume $|\tilde{\psi}_{2D}\rangle$ to be the ground state; our argument applies even if there are edge excitations, as long as the global state is pure.

The key observation that leads to Eq. (13) is the equivalence between the edge and the bulk modular commu-

tator for the set of subsystems shown in Fig. 3(b)):

$$J(A, B, C)|_{\tilde{\psi}_{2D}} = -J(X, Y, Z)|_{\tilde{\psi}_{2D}}. \quad (14)$$

Note that the regions A, B , and C lie at the edge while the regions X, Y , and Z lie entirely in the bulk. Thus, $J(A, B, C)|_{\tilde{\psi}_{2D}}$ is the modular commutator at the edge and $J(X, Y, Z)|_{\tilde{\psi}_{2D}}$ is the modular commutator in the bulk. Once this relation is established, one can use the formula for the bulk modular commutator [5], i.e., $J(X, Y, Z)|_{\tilde{\psi}_{2D}} = -\frac{\pi}{3} \mathfrak{c}_-$ to complete the derivation.

The equivalence of the two modular commutators directly follows from Section VI of Ref. [6], as we explain below. (See SM for a more detailed explanation.) First of all, the state $|\tilde{\psi}_{2D}\rangle$, being indistinguishable from the ground state in the bulk, satisfies the axioms of entanglement bootstrap [10]. Of particular importance to us is the axiom **A1** in Ref. [10], which holds for local disk-like regions away from the edge; it says $(S_{BC} + S_{CD} - S_B - S_D)|_{\psi_{2D}} = 0$ for the green disk BCD shown in Fig. 3(b), where $|\psi_{2D}\rangle$ is the ground state. This axiom, applied to the bulk disk $XYZW$ of Fig. 3(c), gives $I(A' : Y|X) = I(C' : Z|Y) = 0$. It then follows that, for state $|\tilde{\psi}_{2D}\rangle$:

$$J(X, Y, Z) = J(A'X, Y, C'Z) = -J(A'X, WB', C'Z).$$

Letting $A = A'X$, $B = B'W$, and $C = C'Z$, we conclude Eq. (14).

Let us emphasize the generality of the argument above. Note that nowhere in the derivation did we use any symmetry (e.g., translation or rotation symmetry) nor did we use any condition of the state in the vicinity of the edge. For instance, even in the presence of strong disorder, even though the conformal symmetry does not hold — not even approximately — formula (13) still holds; this is numerically verified for integer quantum Hall states, see the SM. Moreover, the argument holds as long as $|\tilde{\psi}_{2D}\rangle = U_{\text{edge}}|\psi_{2D}\rangle$, where U_{edge} is *any* unitary operator along the edge which is thin compared to the width of the subsystems; specifically, U_{edge} should be supported within the annulus $A'B'C'$ for the choice of ABC in Fig. 3(c). (Under a plausible assumption, the unitarity assumption can be dropped. See SM for the detail.)

Holographic interpretation— In the AdS/CFT correspondence [20], entanglement quantities of the boundary CFT are mapped to geometric quantities in the bulk of an asymptotic AdS space. For example, the Ryu-Takayanagi (RT) formula [4] implies that the entanglement entropy of a boundary region A is given by the minimal length of the bulk geodesic γ_A (also known as the RT surface) homologous to the region. Some examples are shown in Fig. 5.

Here we propose to extend the holographic dictionary to the modular commutator. We propose:

$$J(A, B, C) = \frac{\pi \mathfrak{c}_-}{6} \sum_i \cos \theta_i, \quad (15)$$

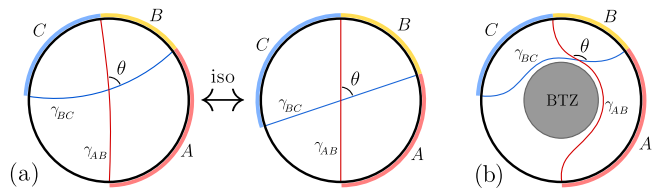


FIG. 5. Verified cases of the holographic conjecture: (a) At zero temperature. Each disk is a Poincaré disk and the two are related by an isometry. (b) At a finite (high) temperature such that $\beta \ll L$.

where $\{\theta_i\}$ is the set of crossing angles of the RT surfaces, i.e., geodesics γ_{AB} and γ_{BC} . Each θ_i is chosen such that γ_{AB} , seen inwardly, lies at the right side of the angle; see Fig. 5 for examples. In general, AB and BC may have multiple connected components; see SM for the relevant discussion.

We can verify the conjecture for a few simple cases shown in Fig. 5. At zero temperature, $2\eta - 1 = \cos \theta$, where θ is the intersection angle for the two RT surfaces. We can apply an isometry of the bulk to place the intersection point of the two geodesics at the center. Then the two geodesics become straight lines with a crossing angle θ . Since the cross ratio η — given by Eq. (9) — is preserved under this isometry, the identity $2\eta - 1 = \cos \theta$ follows from simple trigonometry. Thus, we arrive at

$$J(A, B, C)|_{\Omega} = \frac{\pi \mathfrak{c}_-}{6} \cos \theta. \quad (16)$$

At high temperatures $\beta \ll L$, the CFT is dual to another classical geometry, a BTZ black hole [21] in the bulk; see Fig. 5(b). An analogous derivation applies because the BTZ black hole can be viewed as a quotient of the global AdS₃. The result confirms our conjecture. (See SM for details.)

In AdS/CFT, the dual of the boundary modular Hamiltonian over a region A (denoted as K_A) is known [22]:

$$K_A = \frac{\text{Area}(A)}{4G_N} + K_{\text{bulk}} + o(G_N), \quad (17)$$

where G_N is Newton's constant, $\text{Area}(A)$ is the area operator [23], and K_{bulk} is the modular Hamiltonian of a bulk region enclosed by the RT surface associated with A . Since the leading contribution to the bulk modular Hamiltonian is the area operator, we expect that the dominant contribution comes from the commutator of such operators. While this quantity is zero [24] for a single-time slice when the chiral central charge is zero, our work shows that generally it can be nonzero. In particular, by the standard uncertainty relation, we can conclude

$$\frac{(\Delta \text{Area}(AB))(\Delta \text{Area}(BC))}{G_N^2} \geq \frac{4\pi \mathfrak{c}_-}{3} |\cos \theta|. \quad (18)$$

Thus, for large chiral central charge, the uncertainty in the area can be parametrically large compared to the Planck scale.

Discussion— In this Letter, we computed the modular commutator [5, 6] in 1+1D CFTs, arriving at a simple formula Eq. (1) and discussing its applications in condensed matter systems and holography. For future work, it will be interesting to verify our conjecture in AdS/CFT to more general setups, e.g., disconnected intervals and when a matter field is placed in the bulk. Another interesting open problem is how our conjecture generalizes to higher dimensions. On the condensed matter side, it would be interesting to understand how Eqs. (12) and (13) generalize when the sector of the chiral edge is modified by an anyon in the bulk.

Acknowledgments:— We thank Molly Kaplan, Nima Lashkari, Ruihua Fan, John McGreevy and Dan Rannard for helpful discussions. B.S. is supported by the University of California Laboratory Fees Research Program, grant LFR-20-653926, and the Simons Collaboration on Ultra-Quantum Matter, grant 652264 from the Simons Foundation. Y.Z. is supported by the Q-FARM fellowship at Stanford University. I.L. is supported by a UC Davis Graduate Program Fellowship. J.S. is supported by AFOSR award FA9550-19-1-0369, CIFAR, DOE award DE-SC0019380 and the Simons Foundation.

* These authors contributed equally.

- [1] A. Kitaev and J. Preskill, Topological entanglement entropy, *Phys. Rev. Lett.* **96**, 110404 (2006).
- [2] M. Levin and X.-G. Wen, Detecting topological order in a ground state wave function, *Phys. Rev. Lett.* **96**, 110405 (2006).
- [3] P. Calabrese and J. Cardy, Entanglement entropy and quantum field theory, *Journal of Statistical Mechanics: Theory and Experiment* **2004**, P06002 (2004).
- [4] S. Ryu and T. Takayanagi, Holographic derivation of entanglement entropy from the anti-de sitter space/conformal field theory correspondence, *Phys. Rev. Lett.* **96**, 181602 (2006).
- [5] I. H. Kim, B. Shi, K. Kato, and V. V. Albert, Chiral Central Charge from a Single Bulk Wave Function, *Phys. Rev. Lett.* **128**, 176402 (2022), arXiv:2110.06932 [quant-ph].
- [6] I. H. Kim, B. Shi, K. Kato, and V. V. Albert, Modular commutator in gapped quantum many-body systems (2021), arXiv:2110.10400.
- [7] C. L. Kane and M. P. A. Fisher, Quantized thermal transport in the fractional quantum Hall effect, *Phys. Rev. B* **55**, 15832 (1997), arXiv:cond-mat/9603118 [cond-mat].
- [8] N. Read and D. Green, Paired states of fermions in two dimensions with breaking of parity and time-reversal symmetries and the fractional quantum hall effect, *Phys. Rev. B* **61**, 10267 (2000).
- [9] A. Kitaev, Anyons in an exactly solved model and beyond, *Ann. Phys.* **321**, 2 (2006).
- [10] B. Shi, K. Kato, and I. H. Kim, Fusion rules from entanglement, *Annals of Physics* **418**, 168164 (2020).
- [11] H. Casini, M. Huerta, and R. C. Myers, Towards a derivation of holographic entanglement entropy, *Journal of High Energy Physics* **2011**, 36 (2011), arXiv:1102.0440 [hep-th].
- [12] J. J. Bisognano and E. H. Wichmann, On the duality condition for a hermitian scalar field, *Journal of Mathematical Physics* **16**, 985 (1975), <https://doi.org/10.1063/1.522605>.
- [13] J. J. Bisognano and E. H. Wichmann, On the duality condition for quantum fields, *Journal of Mathematical Physics* **17**, 303 (1976), <https://aip.scitation.org/doi/pdf/10.1063/1.522898>.
- [14] N. Iqbal and A. C. Wall, Anomalies of the entanglement entropy in chiral theories, *Journal of High Energy Physics* **2016**, 111 (2016).
- [15] S. Hellerman, D. Orlando, and M. Watanabe, Quantum Information Theory of the Gravitational Anomaly, arXiv e-prints, arXiv:2101.03320 (2021), arXiv:2101.03320 [hep-th].
- [16] J. Cardy and E. Tonni, Entanglement hamiltonians in two-dimensional conformal field theory, *Journal of Statistical Mechanics: Theory and Experiment* **2016**, 123103 (2016).
- [17] D. Bernard and B. Doyon, Energy flow in non-equilibrium conformal field theory, *Journal of Physics A Mathematical General* **45**, 362001 (2012), arXiv:1202.0239 [cond-mat.str-el].
- [18] H.-H. Tu, Y. Zhang, and X.-L. Qi, Momentum polarization: An entanglement measure of topological spin and chiral central charge, *Phys. Rev. B* **88**, 195412 (2013).
- [19] M. J. Bhaseen, B. Doyon, A. Lucas, and K. Schalm, Energy flow in quantum critical systems far from equilibrium, *Nature Physics* **11**, 509 (2015).
- [20] J. Maldacena, The large-n limit of superconformal field theories and supergravity, *International Journal of Theoretical Physics* **38**, 1113 (1999).
- [21] M. Banados, C. Teitelboim, and J. Zanelli, Black hole in three-dimensional spacetime, *Phys. Rev. Lett.* **69**, 1849 (1992), arXiv:hep-th/9204099 [hep-th].
- [22] D. L. Jafferis, A. Lewkowycz, J. Maldacena, and S. J. Suh, Relative entropy equals bulk relative entropy, *Journal of High Energy Physics* **2016**, 4 (2016).
- [23] D. Harlow, The Ryu-takayanagi formula from quantum error correction, *Communications in Mathematical Physics* **354**, 865 (2017).
- [24] M. Kaplan and D. Marolf, The action of HRT-areas as operators in semiclassical gravity, arXiv e-prints, arXiv:2203.04270 (2022), arXiv:2203.04270 [hep-th].
- [25] E. Witten, Light rays, singularities, and all that, *Reviews of Modern Physics* **92**, 045004 (2020), arXiv:1901.03928 [hep-th].
- [26] J. Cardy and E. Tonni, Entanglement Hamiltonians in two-dimensional conformal field theory, *Journal of Statistical Mechanics: Theory and Experiment* **2016**, 123103 (2016).
- [27] E. H. Lieb and M. B. Ruskai, Proof of the strong subadditivity of quantum-mechanical entropy, *Journal of Mathematical Physics* **14**, 1938 (1973), <https://doi.org/10.1063/1.1666274>.
- [28] D. Petz, Monotonicity of quantum relative entropy revisited, *Reviews in Mathematical Physics* **15**, 79 (2003), arXiv: quant-ph/0209053.
- [29] P. Hayden, R. Jozsa, D. Petz, and A. Winter, Structure of

- States Which Satisfy Strong Subadditivity of Quantum Entropy with Equality, *Communications in Mathematical Physics* **246**, 359 (2004), arXiv:quant-ph/0304007 [quant-ph].
- [30] M. Bañados, M. Henneaux, C. Teitelboim, and J. Zanelli, Geometry of the 2+1 black hole, *Phys. Rev. D* **48**, 1506 (1993), arXiv:gr-qc/9302012 [gr-qc].
- [31] T. Needham, *Visual complex analysis* (Oxford University Press, 1998).
- [32] S. Carlip, TOPICAL REVIEW: The (2 + 1)-dimensional black hole, *Classical and Quantum Gravity* **12**, 2853 (1995), arXiv:gr-qc/9506079 [gr-qc].
- [33] W. Li, W. Song, and A. Strominger, Chiral gravity in three dimensions, *Journal of High Energy Physics* **2008**, 082 (2008), arXiv:0801.4566 [hep-th].
- [34] S. W. Hawking and D. N. Page, Thermodynamics of Black Holes in anti-De Sitter Space, *Commun. Math. Phys.* **87**, 577 (1983).
- [35] E. Witten, Anti-de Sitter space, thermal phase transition, and confinement in gauge theories, *Adv. Theor. Math. Phys.* **2**, 505 (1998), arXiv:hep-th/9803131.
- [36] M. Headrick, Lectures on entanglement entropy in field theory and holography, arXiv e-prints, arXiv:1907.08126 (2019), arXiv:1907.08126 [hep-th].
- [37] I. Peschel and V. Eisler, Reduced density matrices and entanglement entropy in free lattice models, *Journal of Physics A: Mathematical and Theoretical* **42**, 504003 (2009).
- [38] D. R. Hofstadter, Energy levels and wave functions of bloch electrons in rational and irrational magnetic fields, *Phys. Rev. B* **14**, 2239 (1976).
- [39] D. J. Thouless, M. Kohmoto, M. P. Nightingale, and M. den Nijs, Quantized Hall Conductance in a Two-Dimensional Periodic Potential, *Phys. Rev. Lett.* **49**, 405 (1982).
- [40] Q. Niu, D. J. Thouless, and Y.-S. Wu, Quantized hall conductance as a topological invariant, *Phys. Rev. B* **31**, 3372 (1985).
- [41] P. W. Anderson, Absence of diffusion in certain random lattices, *Phys. Rev.* **109**, 1492 (1958).
- [42] K. v. Klitzing, G. Dorda, and M. Pepper, New method for high-accuracy determination of the fine-structure constant based on quantized hall resistance, *Phys. Rev. Lett.* **45**, 494 (1980).
- [43] Q. Zhu, P. Wu, R. N. Bhatt, and X. Wan, Localization-length exponent in two models of quantum hall plateau transitions, *Phys. Rev. B* **99**, 024205 (2019).
- [44] B. Sbierski, E. J. Dresselhaus, J. E. Moore, and I. A. Gruzberg, Criticality of two-dimensional disordered dirac fermions in the unitary class and universality of the integer quantum hall transition, *Phys. Rev. Lett.* **126**, 076801 (2021).
- [45] B. A. Bernevig, *Topological Insulators and Topological Superconductors* (Princeton University Press, 2013).

Appendix A: Geometric derivation for general Cauchy surface

We present a geometric derivation of a formula for the modular commutator for three contiguous intervals lying on a general Cauchy surface. A Cauchy surface is a spacelike hypersurface which generalizes surfaces on a single-time slice.¹ In 1+1D, it represents a spacelike curve, e.g., the ones shown in Fig. 7. For any spacelike curve, we can define a Hilbert space and a quantum state. Since the modular commutator is defined in terms of states, we can define it also for general spacelike curves.

Our formula for the modular commutator reads:

$$J(A, B, C)_{|\Omega_\Sigma\rangle} = \frac{\pi c_L}{6}(2\eta_v - 1) - \frac{\pi c_R}{6}(2\eta_u - 1), \quad (\text{A1})$$

where $\eta_u = \frac{u_{12}u_{34}}{u_{13}u_{24}}$, $\eta_v = \frac{v_{12}v_{34}}{v_{13}v_{24}}$. Here $u = t - x$ and $v = x + t$ are light-cone coordinates and $u_{ij} = u_j - u_i$, $v_{ij} = v_j - v_i$. The indices represent the end points of the intervals A, B , and C ; see Fig. 7. Eq. (A1) is a generalization of the key equation in the main text; see Eq. (1) for comparison.

Two ideas are used to derive Eq. (A1). First, the modular flows for the subsystems we consider correspond to vector fields within their respective domains of dependence (causal diamonds). Thus, the modular flow relates the quantum states on different Cauchy surfaces in a simple way. To that end, we review known facts about modular flow in conformal field theory (CFT) in Section A.1. Second, the modular commutator can be computed by calculating the response of the entanglement entropy against a modular flow. This calculation is explained in Section A.2.

1. Modular flow in CFT

Modular flow is the flow generated by the modular Hamiltonian. Let A be a subregion of some Cauchy surface Σ . The modular Hamiltonian [11, 26] associated with A is $K_A = -\ln \rho_A$, where ρ_A is the reduced density matrix of the given quantum state on A . We shall focus on the vacuum state of the theory throughout this Section.

¹ For an interested reader, here is a more precise definition [25]. A Cauchy surface in M is an achronal spacelike hypersurface Σ with the property that if p is a point in M not in Σ , then every inextendible causal path through p intersects Σ .

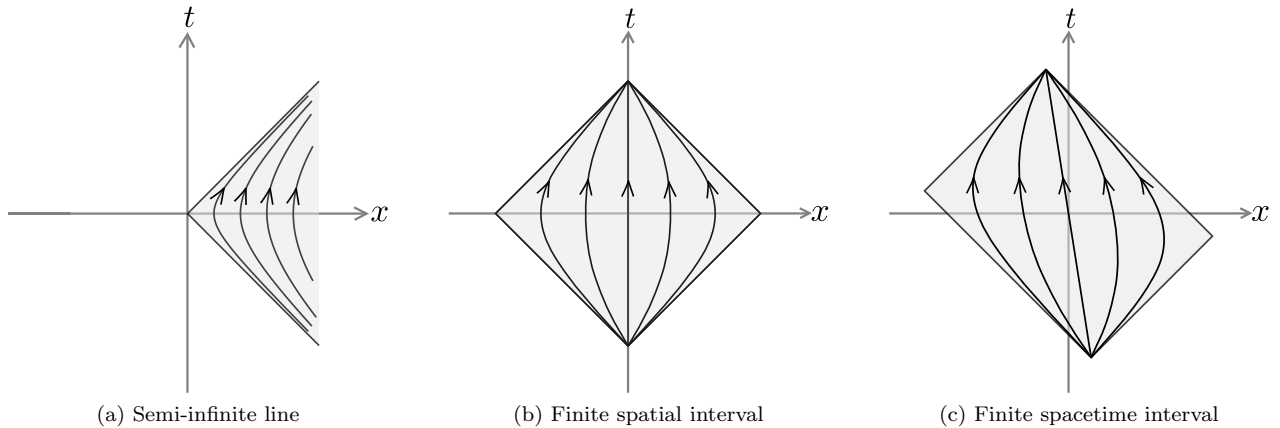


FIG. 6. Causal diamonds that are the domain of dependence of (a) a semi-infinite line, (b) a finite-line on the x -axis, and (c) a general spacelike interval. The modular flow for these cases can be represented as vector fields within the respective causal diamonds.

The modular Hamiltonian generates the following one-parameter evolution of operators within the causal diamond of A :

$$\mathcal{O} \rightarrow U(s)\mathcal{O}U(-s), \quad \text{where} \quad U(s) = \rho_A^{is} = e^{-iK_A s}. \quad (\text{A2})$$

For $s \in \mathbb{R}$, $U(s)$ is unitary. This transformation maps the set of operators in the causal diamond to itself, thus preserving the algebra of operators on A . This map can be generally nonlocal, in the sense that local operators may be mapped to nonlocal operators.

However, for the cases considered below, local operators do get mapped to local operators. Under the modular flow, we obtain $U(s)\mathcal{O}_x U(-s) = \mathcal{O}'_{x(s)}$, where $\mathcal{O}'_{x(s)}$ is an operator at $x(s)$. In fact, if \mathcal{O} is a primary, then \mathcal{O}' is proportional to \mathcal{O} up to a conformal factor [11]. The spacetime point $x(s)$ can be obtained by integrating a vector field $2\pi V_K$ associated with the modular flow with the initial condition $x(0) = x$.

We discuss some examples below, accompanied by Fig. 6 which depicts the vector fields V_K within the causal diamond to represent the modular flow.

Example 1 (Quantum Field theory and semi-infinite line). Let us begin with the case of a semi-infinite line $A = [0, \infty)$. The modular Hamiltonian then becomes $K_A = 2\pi B$, where B is the generator of the boost. The corresponding vector field is

$$V_K = x\partial_t + t\partial_x. \quad (\text{A3})$$

In the light-cone coordinates $u = t - x$ and $v = x + t$, this becomes

$$V_K = -u\partial_u + v\partial_v. \quad (\text{A4})$$

This fact follows from Lorentz invariance alone, and as such, holds for any Lorentz invariant quantum field theory. (The causal diamond for the semi-infinite line is known as the Rindler wedge; see Fig. 6(a) for an illustration.)

Example 2 (1+1D CFT, a single finite interval on the infinite line). Consider a 1+1D CFT on the infinite line and let A be a finite spacetime interval, with endpoints (u_1, v_1) and (u_3, v_3) . These two endpoints can be located on a single-time slice (Fig. 6(b)) or on a boosted interval (Fig. 6(c)). The conformal symmetry guarantees that the modular Hamiltonian is local and can be associated with a vector field V_K . In the light-cone coordinate, we obtain:

$$V_K = -\frac{(u - u_1)(u_3 - u)}{u_{13}}\partial_u + \frac{(v - v_1)(v_3 - v)}{v_{13}}\partial_v, \quad (\text{A5})$$

where $u_{ij} \equiv u_j - u_i$. From Eq. (A5), the expression of V_K in the (x, t) coordinate can be worked out straightforwardly. For the particular case in which the two endpoints of the interval lie on the x axis, with coordinates $(x_1, 0)$ and $(x_3, 0)$, we have

$$V_K = \frac{(x - x_1)(x_3 - x) - t^2}{x_{13}}\partial_t + \frac{t(x_1 + x_3 - 2x)}{x_{13}}\partial_x. \quad (\text{A6})$$

One way to derive Eq. (A5) is to use a conformal map from the Rindler wedge to the finite causal diamond shown in Fig. 6(c):

$$f(u) = \frac{u_1 - u_3 u}{1 - u}, \quad f(v) = \frac{v_1 - v_3 v}{1 - v}. \quad (\text{A7})$$

Note that Eq. (A7) is the analog of fractional linear transformations in the Lorentzian signature.

Let us make a remark on a difference between these two examples, which will be useful in Section A2. The vector field associated with the boost (Example 1) preserves the spacetime volume element inside the Rindler wedge. That is to say, if we take an infinitesimal square-shaped diamond ($dudv$) inside the Rindler wedge, its volume is preserved, even though the square becomes a rectangle. In contrast, the vector field in Example 2 changes the spacetime volume element. This manifests in the fact that the upper half of the causal diamond is squashed under the flow.

2. General Cauchy surface

In quantum field theory, one can choose any Cauchy surface to define a Hilbert space. Let Σ be a Cauchy surface, which separates the spacetime into the past and the future. The “ground state” $|\Omega_\Sigma\rangle$ on the Cauchy surface is defined by the path integral on the spacetime from the past of Σ . We can generalize the result in the main text to contiguous intervals A, B , and C on any Cauchy surface. Let (u_i, v_i) , $i = 1, 2, 3, 4$ be the endpoints of the three intervals (see Fig. 7). (Here we assume that the space direction is infinite.) The key formula we derive in this Section is

$$J(A, B, C)|_{\Omega_\Sigma} = \frac{\pi c_L}{6}(2\eta_v - 1) - \frac{\pi c_R}{6}(2\eta_u - 1), \quad (\text{A8})$$

where

$$\eta_u = \frac{u_{12}u_{34}}{u_{13}u_{24}}, \quad \eta_v = \frac{v_{12}v_{34}}{v_{13}v_{24}}. \quad (\text{A9})$$

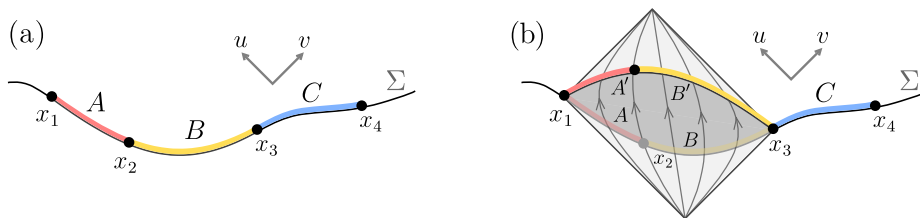


FIG. 7. (a) Three contiguous intervals A, B and C on a general Cauchy surface Σ . (b) The modular flow within the domain of dependence (causal diamond) of AB . The coordinates of the endpoints are $x_i = (u_i, v_i)$.

Remark. Before presenting the derivation, let us remark on the physical implications of Eq. (A8).

- The formula implies that one can determine both c_L and c_R by computing $J(A, B, C)|_{\Omega_\Sigma}$ for the state $|\Omega_\Sigma\rangle$ on a general Cauchy surface Σ . Note that the pair $\{c_L, c_R\}$ contains more information than the chiral central charge of the CFT, $c_- = c_L - c_R$. Since only the latter can be obtained from a computation of $J(A, B, C)|_{\Omega_\Sigma}$ on a single-time slice, a richer set of physical information may be obtained by considering more general Cauchy surfaces.
- Since the Cauchy surface is spacelike, two points close in the v coordinate must be also close in the u coordinate. Therefore, if region B becomes sufficiently small, i.e., $(u_2, v_2) \rightarrow (u_3, v_3)$, or equivalently A and C becomes sufficiently long, i.e., $(u_1, v_1) \rightarrow (-\infty, -\infty), (u_4, v_4) \rightarrow (+\infty, +\infty)$, we get $\eta_u = \eta_v = 1$ and $J(A, B, C) = \pi c_-/6$. In the opposite limit where A or C becomes sufficiently small (or B becomes sufficiently large), we have $\eta_u = \eta_v = 0$ and $J(A, B, C) = -\pi c_-/6$. These are independent of the shape of the Cauchy surface and so is the difference $J(\eta = 1) - J(\eta = 0) = \pi c_-/3$.

In the rest of this Section, we provide a geometric derivation of Eq. (A8), making use of the facts about modular flow discussed in Section A1. Specifically, we make use of the vector field associated with the modular flow; see Eq. (A5). Like in the main text, the modular commutator is given by the response of the entanglement entropy S_{BC} under the modular flow [6], where

$$J(A, B, C)_\rho = - \left. \frac{dS(\rho_{BC}(s))}{ds} \right|_{s=0}, \quad (\text{A10})$$

and

$$\rho_{BC}(s) = \text{Tr}_A(e^{-iK_{AB}s} \rho_{ABC} e^{iK_{AB}s}). \quad (\text{A11})$$

The entanglement entropy of the vacuum of a chiral CFT [14] is

$$S_{BC} = \frac{c_L}{12} \ln \frac{(v_4 - v_2)^2}{\epsilon_{v2}\epsilon_{v4}} + \frac{c_R}{12} \ln \frac{(u_4 - u_2)^2}{\epsilon_{u2}\epsilon_{u4}}. \quad (\text{A12})$$

Here $\epsilon_{u(v)2(4)}$ denotes the UV cutoffs in the u and v directions at the respective endpoints. The UV cutoffs satisfy $\epsilon_{u2}\epsilon_{v2} = \epsilon_2^2$, $\epsilon_{u4}\epsilon_{v4} = \epsilon_4^2$, where $\epsilon_{2(4)}$ is the proper length of the UV cutoff at the two points. Importantly, the cutoffs $\epsilon_{u(v)2(4)}$ transform as null vectors. The change of S_{BC} comes from two contributions: (i) the change of the spacetime point (u_2, v_2) under the flow. (ii) the rescaling of UV cutoffs in light-cone coordinates at the same point (u_2, v_2) ,

$$\frac{dS_{BC}}{ds} = - \left(\frac{c_L}{6} \frac{dv_2/ds}{v_{24}} + \frac{c_L}{12} \frac{d \ln \epsilon_{v2}}{ds} \right) + (v \leftrightarrow u, c_L \leftrightarrow c_R) \quad (\text{A13})$$

Since in the modular flow (Eq. (A5)) u and v coordinates are transformed separately, it follows that $J(A, B, C)$ admits two contributions, one depending only on v and the other depending only on u .

Now let us focus on the v coordinate. (The analysis for the u coordinate works in a similar way.) From the coefficient of ∂_v in Eq. (A5) we read off

$$\left. \frac{dv_2}{ds} \right|_{s=0} = 2\pi \frac{v_{12}v_{23}}{v_{13}}. \quad (\text{A14})$$

In order to compute the rescaling of the UV cutoff, we consider a light-cone segment $[v_2, v_2 + \epsilon_{v2}]$. Under the modular flow, the two endpoints get shifted. In leading order of s and ϵ_{v2} ,

$$v_2 \rightarrow v_2 + s \left(\left. \frac{dv_2}{ds} \right|_{s=0} \right) \quad (\text{A15})$$

and

$$v_2 + \epsilon_{v2} \rightarrow v_2 + \epsilon_{v2} + s \left(\left. \frac{dv_2}{ds} + \epsilon_{v2} \frac{d}{dv_2} \frac{dv_2}{ds} \right|_{s=0} \right). \quad (\text{A16})$$

The length of the segment is the difference of the endpoint, and it gets rescaled to

$$\epsilon_{v2}(s) = \epsilon_{v2} \left(1 + s \frac{d}{dv_2} \frac{dv_2}{ds} \right) \quad (\text{A17})$$

Therefore

$$\frac{d \ln \epsilon_{v2}}{ds} = \frac{d}{dv_2} \frac{dv_2}{ds} = 2\pi \frac{v_{23} - v_{12}}{v_{13}}. \quad (\text{A18})$$

Finally, substituting Eq. (A14) and Eq. (A18) into Eq. (A13) we obtain the v component of Eq. (A8). The u component can be similarly worked out, resulting in an expression in which v is substituted by u , with an overall minus sign. Adding up the two components, we obtain the main result Eq. (A8).

Remark. If the modular flow does not induce a change of the spacetime volume of element $dudv$ on the local patch near (u_2, v_2) , then the change of cutoffs has the following interpretation:

$$d \ln \epsilon_{v2} = -d \ln \epsilon_{u2} = d\chi, \quad (\text{A19})$$

where $d\chi$ is the infinitesimal boost angle that develops at (u_2, v_2) . This formula holds if the modular flow is a boost, as in Fig. 6(a). This is also the case for the modular flow in the finite causal diamond in Fig. 6(b), provided that (u_2, v_2) lies on the x axis. For a general point (u_2, v_2) within the causal diamond depicted in Fig. 6(b) and (c), formula Eq. (A19) no longer holds. However, the change of cutoffs can still be computed with Eq. (A18).

Appendix B: Operator-based derivation

We present an operator-based derivation of an expression for the modular commutator in the main text. Consider a 1+1D conformal field theory (CFT) with chiral central charge $c_- = c_L - c_R$. Let A , B , and C be three contiguous intervals shown in Fig. 8. In the main text we derived

$$J(A, B, C)|_{\Omega} = \frac{\pi c_-}{6}(2\eta - 1), \quad \text{where } \eta = \begin{cases} \frac{x_{12}x_{34}}{x_{13}x_{24}}, & L \rightarrow \infty, \\ \frac{\sin(\pi x_{12}/L) \sin(\pi x_{34}/L)}{\sin(\pi x_{13}/L) \sin(\pi x_{24}/L)}, & L = \text{finite}. \end{cases} \quad (\text{B1})$$

Here $|\Omega\rangle$ is the vacuum state of the CFT and η is the cross ratio on either an infinite line or on a circle. We shall use the convention $x_{ij} \equiv x_j - x_i$. (In the second case, $x_j \in [0, L)$ and $\sin(\pi x_{13}/L)$ has the geometric meaning of the chord distance on a unit circle.)

The modular commutator $J(A, B, C)|_{\Omega} \equiv i\langle\Omega|[K_{AB}, K_{BC}]|\Omega\rangle$ is the commutator of two modular Hamiltonians, where $K_A \equiv -\ln \rho_A$ is the logarithm of the density matrix ρ_A [11, 26]. Our alternative derivation is based on the exact expression for the modular Hamiltonian and the commutators, which is presented below.

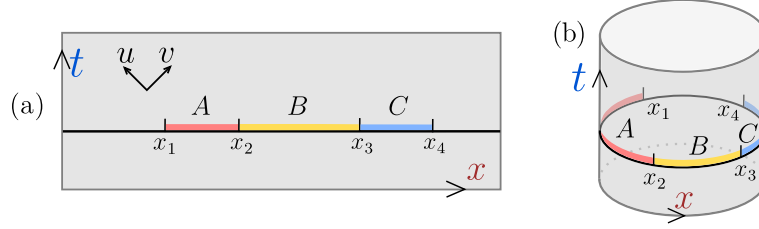


FIG. 8. (a) Three contiguous intervals A , B , and C , on a single-time slice. (b) Contiguous intervals on a circle S^1 with circumference L .

1. On the real line

We first consider the real line. We shall use the choice of subsystems illustrated in Fig. 8(a). The expression for the modular Hamiltonian is [16]

$$K_{AB} = \int_{-\infty}^{\infty} dx f_{AB}(x)(T(x) + \bar{T}(x)), \quad (\text{B2})$$

where

$$f_{AB}(x) = \begin{cases} \frac{(x-x_1)(x_3-x)}{x_{13}} & \text{if } x_1 < x < x_3, \\ 0 & \text{otherwise.} \end{cases} \quad (\text{B3})$$

We can similarly define f_{BC} :

$$f_{BC}(x) = \begin{cases} \frac{(x-x_2)(x_4-x)}{x_{24}} & \text{if } x_2 < x < x_4, \\ 0 & \text{otherwise.} \end{cases} \quad (\text{B4})$$

In order to proceed, we need to compute the commutators $[T(x), T(y)]$ and $[\bar{T}(x), \bar{T}(y)]$. This can be done most easily using the operator product expansion (OPE) of the stress-energy tensor:

$$T(z)T(w) = \frac{c_L/2}{(z-w)^4} - \frac{2T(w)}{(z-w)^2} - \frac{\partial T(w)}{z-w} + \dots, \quad (\text{B5})$$

$$\bar{T}(\bar{z})\bar{T}(\bar{w}) = \frac{c_R/2}{(\bar{z}-\bar{w})^4} - \frac{2\bar{T}(\bar{w})}{(\bar{z}-\bar{w})^2} - \frac{\partial \bar{T}(\bar{w})}{\bar{z}-\bar{w}} + \dots, \quad (\text{B6})$$

where $z = x + i\tau$, $\bar{z} = x - i\tau$ are complex coordinates in Euclidean spacetime. (Note that the second and third term differs from the conventional notation of TT OPE because usually the complex coordinate is defined by $z = \tau + ix$). The commutator can be obtained from

$$[T(x), T(y)] = T(x + i\epsilon)T(y - i\epsilon) - T(y + i\epsilon)T(x - i\epsilon), \quad (\text{B7})$$

$$[\bar{T}(x), \bar{T}(y)] = \bar{T}(x + i\epsilon)\bar{T}(y - i\epsilon) - \bar{T}(y + i\epsilon)\bar{T}(x - i\epsilon), \quad (\text{B8})$$

where $\epsilon > 0$ is infinitesimal. Using the identity

$$\frac{1}{x - y - i\epsilon} - \frac{1}{x - y + i\epsilon} = 2\pi i \delta(x - y) \quad (\text{B9})$$

and its higher order derivatives, one arrives at

$$[T(x), T(y)] = i\frac{\pi c_L}{6}\delta'''(x - y) + 4\pi i T(y)\delta'(x - y) - 2\pi i \partial T(y)\delta(x - y), \quad (\text{B10})$$

$$[\bar{T}(x), \bar{T}(y)] = -i\frac{\pi c_R}{6}\delta'''(x - y) - 4\pi i \bar{T}(y)\delta'(x - y) + 2\pi i \bar{\partial}\bar{T}(y)\delta(x - y), \quad (\text{B11})$$

and $[T(x), \bar{T}(y)] = 0$ follows from the fact that the OPE between T and \bar{T} is regular. Here $\delta'(x - y) \equiv d\delta(x - y)/dx$ and $\delta'''(x - y) \equiv d^3\delta(x - y)/dx^3$ are derivatives of the Dirac delta function $\delta(x - y)$. Alternatively, one may obtain this commutator by expanding $T(x)$ in terms of its Fourier modes and using the Virasoro algebra. Taking expectation value on the vacuum state and using the fact that $\langle T \rangle = \langle \bar{T} \rangle = 0$ on the complex plane, we obtain

$$\boxed{\begin{aligned} \langle [T(x), T(y)] \rangle &= i\frac{\pi c_L}{6}\delta'''(x - y), \\ \langle [\bar{T}(x), \bar{T}(y)] \rangle &= -i\frac{\pi c_R}{6}\delta'''(x - y), \\ \langle [T(x), \bar{T}(y)] \rangle &= 0. \end{aligned}} \quad (\text{B12})$$

Here $\langle \dots \rangle \equiv \langle \Omega | \dots | \Omega \rangle$ is the expectation value of operators on the vacuum state. Then the modular commutator can be computed by carrying out the following integral:

$$J(A, B, C)_{|\Omega} = \frac{\pi(c_R - c_L)}{6} \int dx dy f_{AB}(x) f_{BC}(y) \delta'''(x - y). \quad (\text{B13})$$

Let us emphasize a subtlety in Eq. (B13): the first order derivative $f'_{AB}(x)$ is discontinuous at x_1 and x_3 . In particular, the second order derivative contains the delta function:

$$f''_{AB}(x) = \delta(x - x_1) - \delta(x - x_3) - \frac{2}{x_{13}}\theta(x - x_1)\theta(x_3 - x). \quad (\text{B14})$$

We can now carry out the integration in Eq. (B13) as follows:

$$J(A, B, C)_{|\Omega} = \frac{\pi(c_R - c_L)}{6} \int dx f''_{AB}(x) f'_{BC}(x), \quad (\text{B15})$$

leading to

$$J(A, B, C)_{|\Omega} = \frac{\pi c_-}{6}(2\eta - 1), \quad (\text{B16})$$

where we have defined $c_- = c_L - c_R$ and $\eta = (x_{12}x_{34})/(x_{13}x_{24})$.

2. On a circle

Now we consider the vacuum state on a circle of circumference L ; see Fig. 8(b). Now the modular Hamiltonian becomes [16]

$$K_{AB} = \int_{-\infty}^{\infty} dx f_{AB}(x)(T(x) + \bar{T}(x)), \quad (\text{B17})$$

where

$$f_{AB}(x) = \begin{cases} \frac{L}{\pi} \frac{\sin(\pi(x-x_1)/L) \sin(\pi(x_3-x)/L)}{\sin(\pi x_{13}/L)} & \text{if } x_1 < x < x_3 \\ 0 & \text{otherwise} \end{cases} \quad (\text{B18})$$

Similarly one can obtain K_{BC} . In order to compute the modular commutator, we make use of Eq. (B10) and Eq. (B11). Taking expectation values on the circle and using the Casimir energy

$$\langle T(x) \rangle = - \left(\frac{2\pi}{L} \right)^2 \frac{c_L}{24}, \quad (\text{B19})$$

$$\langle \bar{T}(x) \rangle = - \left(\frac{2\pi}{L} \right)^2 \frac{c_R}{24}, \quad (\text{B20})$$

one obtains

$$\begin{aligned} \langle [T(x), T(y)] \rangle &= i \frac{\pi c_L}{6} \left(\delta'''(x-y) + \left(\frac{2\pi}{L} \right)^2 \delta'(x-y) \right), \\ \langle [\bar{T}(x), \bar{T}(y)] \rangle &= -i \frac{\pi c_R}{6} \left(\delta'''(x-y) + \left(\frac{2\pi}{L} \right)^2 \delta'(x-y) \right). \end{aligned} \quad (\text{B21})$$

Then the modular commutator becomes

$$J(A, B, C)_{|\Omega\rangle} = \frac{\pi(c_R - c_L)}{6} \int_0^L dx dy f_{AB}(x) f_{BC}(y) \left(\delta'''(x-y) + \left(\frac{2\pi}{L} \right)^2 \delta'(x-y) \right). \quad (\text{B22})$$

Again taking care of the fact that $f_{AB}(x)$ and $f_{BC}(y)$ are singular at the entangling boundaries and doing the integral, one obtains Eq. (B16) with a redefinition of the cross ratio

$$\eta = \frac{\sin(\pi x_{12}/L) \sin(\pi x_{34}/L)}{\sin(\pi x_{13}/L) \sin(\pi x_{24}/L)}. \quad (\text{B23})$$

Note that another way to obtain this formula is to use the exponential conformal map from the cylinder to the complex plane. The point x_i on the cylinder gets mapped to $z_i = e^{i2\pi x_i/L}$ on the unit circle, and the usual cross ratio $(z_{12}z_{34})/(z_{13}z_{24})$ is exactly Eq. (B23).

Appendix C: Topological invariance: bulk and edge of 2+1D topological orders

We present the details on an information-theoretic argument used in the main text. For concreteness, we assume that the system is on a 2D disk, with an edge. On the ground state $|\psi_{2D}\rangle$ we assume the two axioms of entanglement bootstrap [10]; see Fig. 9.

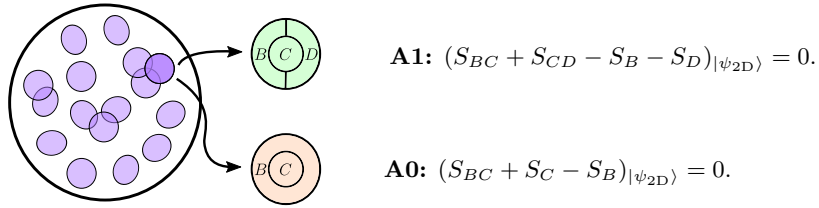


FIG. 9. The physical system on a disk and the two bulk-axioms (**A0** and **A1**) of entanglement bootstrap.

These axioms are applicable when the entanglement area law [1, 2] of 2+1D gapped system holds. For systems with a gapless edge — which is of interests to us — the area law is expected to hold when the regions are separated from the edge by an amount large compared to the bulk correlation length.²

² For realistic systems, especially those with ungappable edges, we expect the area law to have correction which decays exponentially when the subsystems we pick are large compared to the correlation length. We drop these corrections in this Section, assuming these errors will not affect the analysis.

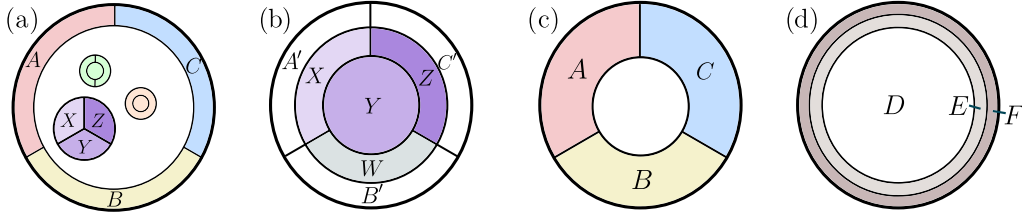


FIG. 10. A 2+1D gapped chiral system on a disk and various choices of subsystems. (a) ABC is an annulus covering the entire edge. The sizes for subsystems are large compared to the bulk correlation length. (b) A different partition of the disk, where $XYZW$ is a bulk disk. (c) Relabeling of regions in (b) as $A = A'X$, $B = B'W$, $C = C'Z$. (d) A finer partition of the annulus covering the edge; here $EF = A'B'C'$.

Proposition 3. *The following statements about $J(A, B, C)$ are true:*

1. $J(A, B, C)|_{\psi_{2D}}$ is invariant under any bulk-deformation of the regions A, B, C . Here a bulk deformation is a “smooth” deformation that preserves the topology of the union of any regions and does not add (or remove) any sites near the edge.

2. For the subsystems shown in Fig. 10(a),

$$J(A, B, C)|_{\psi_{2D}} = -J(X, Y, Z)|_{\psi_{2D}}, \quad (C1)$$

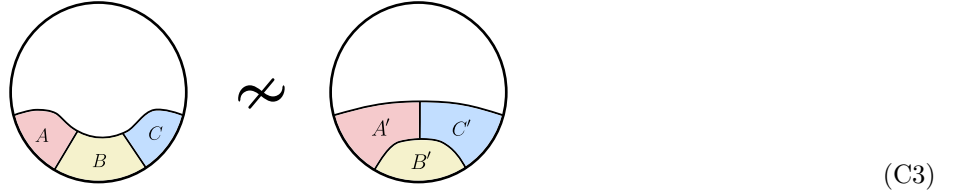
3. Let $|\tilde{\psi}_{2D}\rangle := U_{\text{edge}}|\psi_{2D}\rangle$, where U_{edge} is an arbitrary unitary operator supported on $A'B'C'$ of Fig. 10(b). Then

$$J(A, B, C)|_{\tilde{\psi}_{2D}} = J(A, B, C)|_{\psi_{2D}}. \quad (C2)$$

4. Let $|\tilde{\psi}_{2D}\rangle := \lambda \cdot O_{\text{edge}}|\psi_{2D}\rangle$, where O_{edge} is an operator supported near the edge, on region F (a finer subset of $A'B'C'$); see Fig. 10(d). O_{edge} does not annihilate $|\psi_{2D}\rangle$, and λ is a constant which normalizes the state. Then $J(A, B, C)|_{\tilde{\psi}_{2D}} = J(A, B, C)|_{\psi_{2D}}$.

Remark. A few remarks are in order.

1. The first statement in Proposition 3 does not imply any equality of the modular commutator of the following two configurations:



These two configurations ABC and $A'B'C'$ cannot be smoothly deformed into each other. Indeed, the modular commutators for these two choices of regions are not equal, in general.

2. The second statement essentially follows from the analysis in Section VI of [6].

3. While axiom **A1** is used in all the statements, axiom **A0** is used only in the proof of the fourth statement.

Here are the mathematical facts that will be relevant for our derivation. We define the conditional mutual information as $I(X : Z|Y)_\rho := S(\rho_{XY}) + S(\rho_{YZ}) - S(\rho_Y) - S(\rho_{XYZ})$. Strong subadditivity (SSA) [27] refers to the statement that $I(X : Z|Y)_\rho \geq 0$ for any tripartite state ρ_{ABC} . Petz showed that $I(X : Z|Y)_\rho = 0$ if and only if $\ln \rho_{XYZ} = \ln \rho_{XY} + \ln \rho_{YZ} - \ln \rho_Y$ [28]. For later convenience, we introduce notation $K_X \equiv -\ln \rho_X$ for the modular Hamiltonian. Petz’s result can then be written as

$$I(X : Z|Y)_\rho = 0 \quad \Leftrightarrow \quad K_{XYZ} = K_{XY} + K_{YZ} - K_Y. \quad (C4)$$

An immediate consequence is that

$$I(X : Z|Y)_\rho = 0 \quad \Rightarrow \quad J(X, Y, Z)_\rho = 0. \quad (C5)$$

For any bipartite pure state, $\ln \rho_X |\Psi_{XY}\rangle = \ln \rho_Y |\Psi_{XY}\rangle$, where ρ_X and ρ_Y are the reduced density matrices of $|\Psi_{XY}\rangle$. Another useful equality is $i\langle [K_{AB}, K_A] \rangle = 0$ for any mixed state ρ_{AB} , that is if one subsystem is part of the other subsystem then the modular commutator vanishes. This is because $\text{Tr}(\rho_{AB}[K_{AB}, K_A]) = \text{Tr}([\rho_{AB}, K_{AB}]K_A)$ using the cyclic property of trace. Moreover, the following lemma is useful.

Lemma 4. *The following statements about modular commutator are true.*

1. If ρ_{aABC} satisfies $I(a : B|A) = 0$, then $J(aA, B, C) = J(A, B, C)$.
2. If ρ_{ABbC} satisfies $I(A : b|B) = I(C : b|B) = 0$, then $J(A, bB, C) = J(A, B, C)$.

Proof. First, we prove the first statement. $I(a : B | A) = 0$ implies $K_{aAB} = K_{aA} + K_{AB} - K_A$. Therefore,

$$\begin{aligned} J(aA, B, C) &= i\langle [K_{aAB}, K_{BC}] \rangle \\ &= i\langle [K_{aA} + K_{AB} - K_A, K_{BC}] \rangle \\ &= i\langle [K_{AB}, K_{BC}] \rangle \\ &= J(A, B, C). \end{aligned} \tag{C6}$$

Next, we prove the second statement. By $I(A : b | B) = I(C : b | B) = 0$, we have

$$\begin{aligned} K_{ABb} &= K_{AB} + K_{Bb} - K_B \\ K_{CBb} &= K_{CB} + K_{Bb} - K_B. \end{aligned} \tag{C7}$$

Using these two equations to replace bigger chunks of modular Hamiltonians by small ones supported on the marginals, we get

$$\begin{aligned} J(A, Bb, C) &= i\langle [K_{ABb}, K_{BCb}] \rangle \\ &= i\langle [K_{AB} + K_{Bb} - K_B, K_{BC} + K_{Bb} - K_B] \rangle \\ &= i\langle [K_{AB}, K_{BC}] \rangle + i\langle [K_{AB}, K_{Bb}] \rangle + i\langle [K_{Bb}, K_{BC}] \rangle \\ &\quad - i\langle [K_{AB}, K_B] \rangle - i\langle [K_{Bb}, K_B] \rangle - i\langle [K_B, K_{BC}] \rangle - i\langle [K_B, K_{Bb}] \rangle \\ &= i\langle [K_{AB}, K_{BC}] \rangle \\ &= J(A, B, C) \end{aligned}$$

Two of the three terms in the third line, namely $i\langle [K_{AB}, K_{Bb}] \rangle$ and $i\langle [K_{Bb}, K_{BC}] \rangle$ vanish upon using Eq. (C5). Terms in the fourth line, e.g., $i\langle [K_B, K_{BC}] \rangle$ and $i\langle [K_B, K_{Bb}] \rangle$ vanish because B is a subsystem of BC and Bb . \square

Proof of Proposition 3. First, we prove the invariance under deformations of the bulk. Because of the symmetry of the modular commutator $J(X, Y, Z) = -J(Z, Y, X)$, it suffices to consider the bulk deformations shown in Fig. 11. In total, there are 5 cases.

- For (a), we wish to show $J(aA, B, C) = J(A, B, C)$. This is verified by realizing $I(a : B|A) = 0$ and using Lemma 4.
- For (b), we wish to show $J(aA, B \setminus a, C) = J(A, B, C)$. To derive this identity, we use the fact that $|\psi_{ABCD}\rangle$ is pure to convert the problem into showing $J(aA, D, C) = J(A, D, C)$, which we already solved in (a).
- For (c), we wish to show $J(A, Bb, C) = J(A, B, C)$. The bulk axiom **A1** implies that $I(b : A|B) = I(b : C|B) = 0$. The identity then follows immediately from Lemma 4.
- For (d), we wish to show $J(aA, B, C) = J(A, B, C)$. Using the purity of $|\psi_{ABCD}\rangle$, we can convert the problem into the identity $J(D, C, B) = J(D \setminus a, C, B)$. This follows from Lemma 4 and $I(a : C|D \setminus a) = 0$.
- For (e), we wish to show $J(A, Bb, C) = J(A, B, C)$. Using purity, we convert the problem into showing $J(D \setminus b, C, Bb) = J(D, C, B)$. This follows from $I(b : C|D \setminus b) = I(b : C|B) = 0$ and using Lemma 4 twice.

Second, we prove Eq. (C1), where ABC and XYZ are shown in Fig. 10(a). Importantly, ABC is an annulus covering the entire annulus and XYZ is a bulk disk. For the bulk disk, the modular commutator $J(X, Y, Z)|_{\psi_{2D}}$ is invariant under deformations of the regions within the bulk [5, 6]. For the annulus ABC , we have proved above the analogous invariance under bulk-deformations of ABC . Therefore, for proving Eq. (C1), we can instead consider the

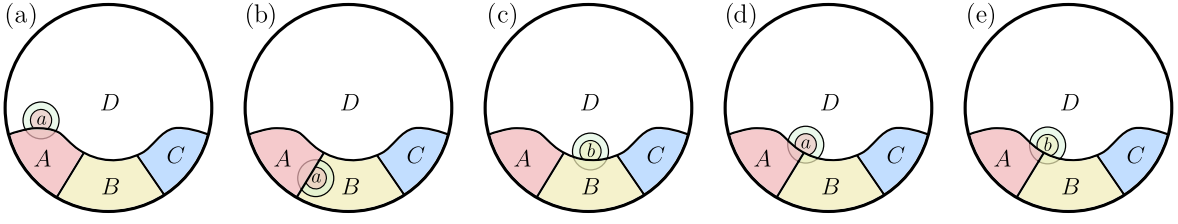


FIG. 11. Bulk-deformations. Each case is verified using axiom **A1** on a bulk disk.

subsystems XYZ and ABC shown in Fig. 10(b) and (c). (Note that these subsystems are different from the ones shown in Fig. 10(a).)

Note that $I(A' : Y|X)|_{\psi_{2D}} = I(C' : Y|Z)|_{\psi_{2D}} = 0$. This is because

$$\begin{aligned} I(A' : Y|X)|_{\psi_{2D}} &= (S_{XY} + S_{YZW} - S_X - S_{ZW})|_{\psi_{2D}} - I(B'C' : Y|ZW)|_{\psi_{2D}} \\ &\leq (S_{XY} + S_{YZW} - S_X - S_{ZW})|_{\psi_{2D}} \\ &= 0. \end{aligned} \quad (\text{C8})$$

In the first line, we use the purity of the state; in the second line, the inequality follows from SSA. For deriving the third line, the important fact is that $XYZW$ is a disk away from the edge. Therefore, one can apply the bulk-axiom **A1**. However, by SSA, the conditional mutual information is always non-negative, $I(A' : Y|X)|_{\psi_{2D}} \geq 0$. Thus, we conclude that $I(A' : Y|X)|_{\psi_{2D}} = 0$. A similar argument leads to $I(C' : Y|Z)|_{\psi_{2D}} = 0$.

Using Lemma 4 and the purity of the global state, we find that:

$$J(X, Y, Z)|_{\psi_{2D}} = J(A'X, Y, C'Z)|_{\psi_{2D}} = -J(A, B, C)|_{\psi_{2D}}. \quad (\text{C9})$$

To prove the third statement of Proposition 3, we observe that all the steps that lead to Eq. (C9) can still go through as long as the area law in the bulk disk $XYZW$ holds. Therefore, $J(X, Y, Z)|_{\tilde{\psi}_{2D}} = -J(A, B, C)|_{\tilde{\psi}_{2D}}$. Because U_{edge} is supported within $A'B'C'$, $|\tilde{\psi}_{2D}\rangle$ and $|\psi_{2D}\rangle$ must have identical reduced density matrix on the disk $XYZW$. Thus, $J(X, Y, Z)|_{\psi_{2D}} = J(X, Y, Z)|_{\tilde{\psi}_{2D}}$. Therefore, $J(A, B, C)|_{\psi_{2D}} = J(A, B, C)|_{\tilde{\psi}_{2D}}$. This completes the proof of Eq. (C2).

Lastly, we prove the fourth statement of Proposition 3. It is crucial to use axiom **A0** here. Axioms **A0** and **A1** for disks of bounded radii (Fig. 9) imply that the same conditions hold on larger regions. Therefore, we can apply the enlarged version of **A0** on the bulk disk DE in Fig. 10(d). The condition reads,

$$(S_{DE} + S_D - S_E)|_{\psi_{2D}} = 0 \implies I(D : F|E)|_{\psi_{2D}} = 0. \quad (\text{C10})$$

A pure state with zero conditional mutual information has the following structure decomposition [29]:

$$|\psi_{2D}\rangle = |\psi_{DE_L}\rangle \otimes |\psi_{E_R F}\rangle. \quad (\text{C11})$$

Here the labels E_L and E_R are associated with a decomposition of Hilbert space $\mathcal{H}_E = (\mathcal{H}_{E_L} \otimes \mathcal{H}_{E_R}) \oplus \dots$. (Note, E_L and E_R are not labels for subsystems of the underlying lattice of the quantum system, unless the state is a product state.) Thus, any operator acting on F will not change the reduced density matrix on D . In fact, $O_F|\psi_{2D}\rangle = \mu U_{EF}|\psi_{2D}\rangle$ for some real number μ and unitary operator U_{EF} . When $\mu \neq 0$, letting $\lambda = 1/\mu$, we find $\lambda O_{\text{edge}}|\psi_{2D}\rangle = U_{\text{edge}}|\psi_{2D}\rangle$. Then statement 4 follows from statement 3. \square

Appendix D: Geometric properties of 2+1D AdS spacetime and BTZ black hole

We review various geometric properties of 2+1 dimensional AdS spacetime (AdS_3) and the BTZ black hole [21, 30]. The focus is on facts related to the crossing angles of spacelike geodesics anchored at the conformal boundary. Symmetry considerations can simplify the problem, as AdS_3 is a maximally symmetric spacetime and the BTZ black hole solution is a quotient of AdS_3 . Specific coordinates are discussed in parallel so that geometric intuitions may be translated into concrete calculations.

1. The global AdS₃ spacetime and crossing angles between geodesics

The global AdS₃ is the simplest vacuum solution of the 2+1D Einstein gravity with a negative cosmological constant. It is a maximally symmetric spacetime. This means that there is an isometry of the spacetime to map a spacetime point q to any point p . a further spacetime rotation can then take the local frame at q to any frame at p , provided that the two frames have the same handedness.

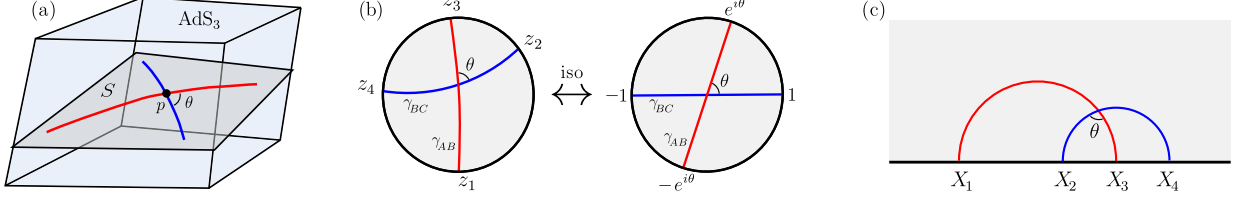


FIG. 12. (a) AdS₃ spacetime with a spacelike hypersurface S passing through point p . Two geodesics contained in S cross each other at p with crossing angle θ . (b) The Poincaré disk model of hyperbolic plane S and an isometry. (c) The upper half-plane model of S .

There are several global coordinates for AdS₃, each making a subset of the symmetry manifest. One is

$$ds^2 = R^2(-\cosh^2 \rho dt^2 + d\rho^2 + \sinh^2 \rho d\phi^2), \quad (\text{D1})$$

where $t \in (-\infty, \infty)$, $\rho \in [0, \infty)$, $\phi \in [0, 2\pi)$, and R is the curvature radius of AdS₃. This is the coordinate system we use in the ensuing discussion. Consider a spacetime point p and a timelike tangent vector at p . They uniquely determine a spacelike hypersurface (S) which passes through p and contains all geodesics orthogonal to the given tangent vector. Geodesics of the global AdS₃ that are tangent to S must stay in it. We shall be interested in a pair of geodesics in S which crosses each other with a crossing angle θ , see Fig. 12(a). To find an explicit coordinate of S , we put p to the origin, and choose the timelike vector be ∂_t in the coordinate system in Eq. (D1). Then S becomes the hypersurface $t = 0$, with the metric

$$ds^2 = R^2(d\rho^2 + \sinh^2 \rho d\phi^2). \quad (\text{D2})$$

The metric in Eq. (D2) describes the hyperbolic plane. The hyperbolic plane is unbounded and it does not have a boundary. However, it has a “conformal boundary”. (This is related to the fact that AdS₃ is not globally hyperbolic and S is not a Cauchy surface.) The conformal boundary can be seen explicitly in the Poincaré disk model, whose metric in complex coordinate is [31]

$$ds^2 = 4R^2 \frac{dzd\bar{z}}{(1-|z|^2)^2}, \quad |z| < 1. \quad (\text{D3})$$

Note that the unit circle $|z| = 1$ is not part of the hyperbolic plane and this is exactly where the conformal boundary (that the dual CFT lives in) is located. The relation between the two sets of coordinates is $\sinh \rho = 2|z|/(1-|z|^2)$ and $\phi = \arg z$.

Geodesics of the Poincaré disk are circular arcs (or straight lines) perpendicular to the boundary $|z| = 1$. Because the metric is proportional to $dzd\bar{z}$ of the complex plane, the apparent crossing angles in the complex plane are identical to the geometric crossing angles. Every isometry of the hyperbolic plane is represented by a fractional linear transformation that keeps the unit circle,

$$z \rightarrow e^{i\alpha} \frac{z - \xi}{1 - \xi z}, \quad (\text{D4})$$

where $\alpha \in [0, 2\pi)$ and $|\xi| < 1$ is a complex number. This constitutes the isometry group $SL(2, R)$ of the hyperbolic plane. As is well-known, this transformation leaves complex cross ratios $\eta_{\text{complex}} \equiv (z_{12}z_{34})/(z_{13}z_{24})$ invariant, where z_j 's are points on the complex plane. If z_1, z_2, z_3 and z_4 are 4 points on the unit circle, then the cross ratio η_{complex} becomes real, and it is identical with the one defined in terms of the chord distance

$$\eta = \frac{\sin(\phi_{12}/2) \sin(\phi_{34}/2)}{\sin(\phi_{13}/2) \sin(\phi_{24}/2)}, \quad (\text{D5})$$

where $\phi_i = \arg z_i$. Using the fractional linear transformation, it is always possible to send the crossing point to the center of the disk. Then the two geodesics become straight lines and the four points are mapped to two pairs of antipodal points; see Fig. 12(b). Then it follows from a simple trigonometry calculation that

$$\cos \theta = 2\eta - 1, \quad \text{where } \eta \text{ is given by Eq. (D5),} \quad (\text{D6})$$

as claimed in the main text.³

We note that there is yet another coordinate, which will be useful in Section D 2. We apply a fractional linear transformation to transform the unit disk to the upper half-plane (see Fig. 13(c)),

$$z = \frac{w - i}{w + i}, \quad (\text{D8})$$

where $w = X + iY$ with $Y > 0$. In this planar coordinate (X, Y) , the metric becomes

$$ds^2 = \frac{R^2}{Y^2}(dX^2 + dY^2). \quad (\text{D9})$$

In this coordinate, the geodesics become semicircles or straight lines perpendicular to the boundary. (The boundary is at $Y = 0$, union with the infinity, is the conformal boundary of the hyperbolic plane.) One can easily verify

$$\cos \theta = 2\eta - 1, \quad \text{where } \eta = \frac{X_{12}X_{34}}{X_{13}X_{24}}. \quad (\text{D10})$$

Here X_j are the X coordinates of the four endpoints and $X_{ij} \equiv X_j - X_i$.

2. Crossing angles and the BTZ black hole

The BTZ black hole is a class of solutions in 2+1D Einstein gravity with a negative cosmological constant [21, 30]. These solutions are labeled by the black hole mass M ($M > 0$) and the angular momentum. Importantly, the solutions can be viewed as a quotient of the global AdS_3 [32]. We shall be interested in the non-rotating solutions whose angular momentum is zero. (The BTZ black hole remains a classical solution to a 2+1D ‘‘chiral gravity’’ theory [33]. In such theories, a gravitational Chern-Simons term is added into the action. It is a way to have a dual boundary CFT that is chiral. The mass and angular momentum of the BTZ black holes are shifted according to the coefficient of the gravitational Chern-Simons term. Below, the mass M always refers to the unshifted one defined directly from the metric.) The ‘‘Schwarzschild coordinate’’ of this solution is given by

$$ds^2 = -\frac{(r^2 - r_+^2)}{R^2} dt^2 + \frac{R^2}{r^2 - r_+^2} dr^2 + r^2 d\phi^2, \quad t \in (-\infty, +\infty), \quad r \in (0, +\infty), \quad \phi \in [0, 2\pi), \quad (\text{D11})$$

where $r_+ = \sqrt{MR}$ is the black hole horizon. This coordinate is valid for $r > 0$ although it has a coordinate singularity at $r = r_+$.

We shall be interested in the $t = 0$ slice outside of the BTZ bulk hole, for $r \geq r_+$. The metric for this single-time slice is $ds^2 = \frac{R^2}{r^2 - r_+^2} dr^2 + r^2 d\phi^2$. The following coordinate transformation⁴

$$X = \frac{\sqrt{r^2 - r_+^2}}{r} \exp(\sqrt{M}\phi) \quad \text{and} \quad Y = \frac{r_+}{r} \exp(\sqrt{M}\phi) \quad (\text{D14})$$

³ In fact, this identity can be verified explicitly using the coordinate (D2) as well, making use of the explicit geodesic solution

$$\gamma_{AB} : \tanh \rho \cos\left(\phi - \frac{\phi_1 + \phi_3}{2}\right) = \cos\left(\frac{\phi_{13}}{2}\right). \quad (\text{D7})$$

⁴ Isometry map of the spacetime outside the horizon to the upper-half space

$$ds^2 = \frac{R^2}{Y^2}(-dT^2 + dX^2 + dY^2). \quad (\text{D12})$$

is also known explicitly [32]. The transformation is

$$T = \frac{\sqrt{r^2 - r_+^2}}{r} \sinh\left(\frac{r_+}{R^2} t\right) \exp(\sqrt{M}\phi), \quad X = \frac{\sqrt{r^2 - r_+^2}}{r} \cosh\left(\frac{r_+}{R^2} t\right) \exp(\sqrt{M}\phi), \quad Y = \frac{r_+}{r} \exp(\sqrt{M}\phi). \quad (\text{D13})$$

identifies this single-time slice as a subset of the upper half-plane

$$ds^2 = \frac{R^2}{Y^2}(dX^2 + dY^2), \quad (\text{D15})$$

where $X \geq 0$ and $Y > 0$.

Let $w = X + iY$, similar to the construction in the last part of Section D 1. The spacetime points of interest is the intersection of the circular strip defined by $|w| \in [1, \exp(2\pi\sqrt{M})]$ and $X \geq 0$, as shown in Fig. 13(b). The identification $\phi \sim \phi + 2\pi$ corresponds to identifying points up to a dilation $(X, Y) \sim \lambda(X, Y)$ where $\lambda = \exp(2\pi\sqrt{M})$. The rotation $\phi \rightarrow \phi + \alpha$ in coordinate (D11) corresponds to dilation $(X, Y) \rightarrow \exp(\alpha\sqrt{M})(X, Y)$ of the upper half-plane. The boundary at the infinity (topologically a circle S^1) is mapped to the interval $[1, \exp(2\pi\sqrt{M})]$ of the X axis, where the two endpoints of the interval are identified. The horizon is at $X = 0$. Two geodesics homologous to boundary intervals are therefore represented as circular arcs perpendicular to the boundary. Note that these geodesics cannot touch the horizon.

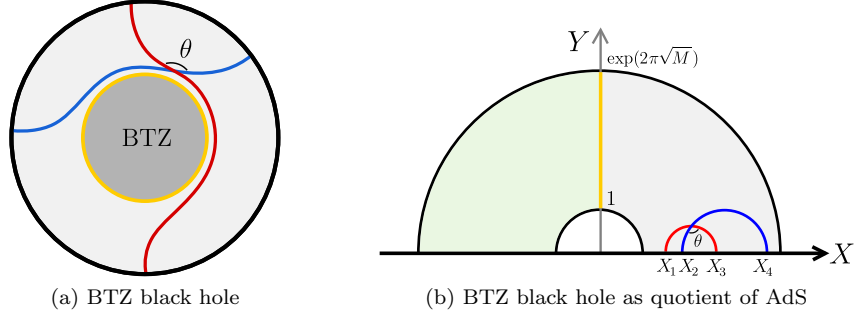


FIG. 13. A single-time slice of the BTZ black hole geometry outside the horizon. (a) The red and blue lines represent geodesics. The yellow circle represents the horizon. The boundary at infinity is the black circle. Unlike the Poincaré disk, the apparent crossing angle here does not faithfully represent the geometric crossing angle. (b) Embedding into the upper half-plane. The inner semicircle and the outer semicircle are identified. The green region on the left of the horizon (yellow) is the other side of the two-sided Kruskal-like extension of the BTZ black hole (outside the horizon).

The crossing angle of the pair of geodesics shown in Fig. 13 can therefore be computed using the parameters in the upper half-plane model in the same manner as Eq. (D10). We write

$$\cos \theta = 2\eta_{\text{eff}} - 1, \quad \text{where} \quad \eta_{\text{eff}} = \frac{X_{12}X_{34}}{X_{13}X_{24}}, \quad (\text{D16})$$

as claimed in the main text⁵. Note that η_{eff} is the “effective” cross ratio, when we think of the region as part of the global hyperbolic plane; it is *not* the cross ratio one defines from the boundary circle. To write η_{eff} in terms of the parameters $x_i \in [0, L)$ of the boundary circle, we rewrite

$$X_j = \exp\left(\frac{2\pi\sqrt{M}x_j}{L}\right) \Rightarrow \eta_{\text{eff}} = \frac{\sinh\left(\frac{\pi\sqrt{M}x_{12}}{L}\right) \sinh\left(\frac{\pi\sqrt{M}x_{34}}{L}\right)}{\sinh\left(\frac{\pi\sqrt{M}x_{13}}{L}\right) \sinh\left(\frac{\pi\sqrt{M}x_{24}}{L}\right)}. \quad (\text{D18})$$

Finally, we relate the classical geometry of BTZ black hole to the boundary CFT assuming the dictionary of AdS/CFT [20]. This duality is available if the CFT is holographic and the temperature is sufficiently high such that the inverse temperature $\beta = 1/T$ satisfies $\beta \ll L$. The mass of the BTZ black hole is expressed as $\sqrt{M} = L/\beta$. We thus find

$$\eta_{\text{eff}} = \frac{\sinh(\pi x_{12}/\beta) \sinh(\pi x_{34}/\beta)}{\sinh(\pi x_{13}/\beta) \sinh(\pi x_{24}/\beta)}. \quad (\text{D19})$$

⁵ Alternatively, one may explicitly compute the crossing angle using the geodesic in the $(\rho, \tilde{\phi})$ coordinate, where $r = r_+ \cosh \rho$, $\tilde{\phi} = r_+ \phi / R$. In this coordinate, the metric of the BTZ black hole is $ds^2 = R^2 \left(-\frac{r_+^2}{R^2} \sinh^2 \rho dt^2 + d\rho^2 + \cosh^2 \rho d\tilde{\phi}^2 \right)$. It is readily seen that this is equivalent to “Euclidean AdS₃” by changing $t \rightarrow i\tilde{\phi}$, $\phi \rightarrow ir_+ t / R$ in Eq. (D1). The geodesic takes on a similar form as in pure AdS,

$$\gamma_{AB} : \tanh \rho \cosh\left(\frac{\tilde{\phi}_{13}}{2}\right) = \cosh\left(\tilde{\phi} - \frac{\tilde{\phi}_1 + \tilde{\phi}_3}{2}\right). \quad (\text{D17})$$

Computing the crossing angles we reach the same conclusion.

Appendix E: Beyond contiguous intervals

In this Section we continue to examine the holographic proposal that we put forward in the main text. In particular, we discuss what happens if there are more than one crossing angles. For instance, consider the examples in Fig. 14(b) and (c), wherein the RT surfaces homologous to the boundary regions AB and BC (denoted as γ_{AB} and γ_{BC} respectively) cross each other at two points.

We conjecture that the contributions from each crossing angle are additive. Specifically, suppose the boundary CFT is dual to a semiclassical bulk geometry and the RT surfaces intersect at a set of crossing angles $\{\theta_i\}$. We conjecture that

$$J(A, B, C) = \frac{\pi c_-}{6} \sum_i s_i \cos \theta_i. \quad (\text{E1})$$

Here $s_i = \pm 1$ are introduced to fix the sign convention. Let us explain the rule for assigning s_i to angle θ_i . If the angle θ_i has geodesic γ_{AB} on its right from an inward-looking point of view, we assign $s_i = 1$; otherwise, $s_i = -1$.

Let us make a few side remarks. First, we only need to pick one crossing angle (out of the four) at each intersection point. It does not matter which angle we pick, because any such choice give the correct answer, due to the sign convention s_i . This prescription automatically ensures that $J(A, B, C) = -J(C, B, A)$, which is a property that must hold generally for the modular commutator. Secondly, one may ask what happens if the geodesics do not share a plane and therefore do not intersect. This can happen for more interesting choices of intervals of the boundary theory, such as those on a general Cauchy surface discussed in Section A. We believe that the conjecture can be generalized to that setup, and we leave this to future investigation.

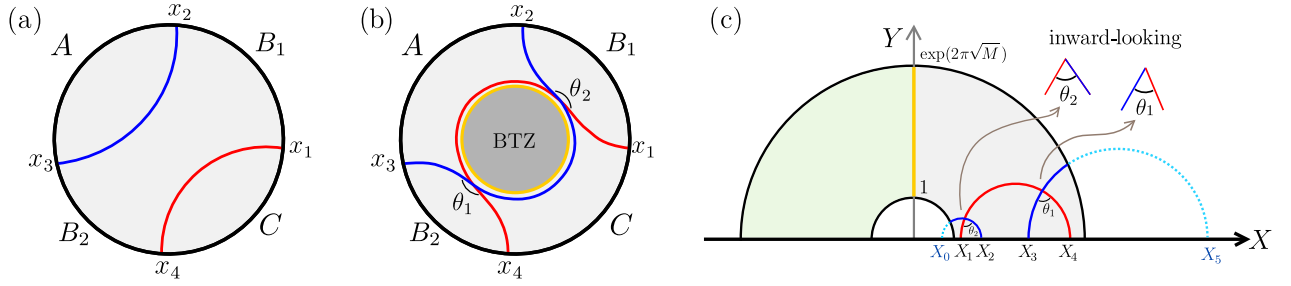


FIG. 14. The boundary circle is partitioned into ABC where B is the union of disjoint intervals B_1 and B_2 . (a) In pure AdS, the two geodesics (γ_{AB} and γ_{BC}) have no intersection. (b) For the BTZ black hole geometry, the two geodesics intersect at two places. (c) Embedding of the region in the upper half-plane. The angles θ_1 and θ_2 are represented accurately. They can be calculated from $\{X_i\}_{i=0}^5$.

As a warmup, let us first consider the pure AdS case with the subsystems A , B , and C covering the entire boundary. We choose B to be a union of two disjoint intervals, denoted as B_1 and B_2 ; see Fig. 14(a). In the Poincaré disk model, it is evident that the two geodesics ending on disjoint boundary intervals (A and C) cannot intersect. Furthermore, geodesics γ_{AB} and γ_C are identical since, on a (global) hyperbolic plane, two points determine a unique geodesic. Similarly, γ_A is identical to γ_{BC} for the same reason. Thus, according to our holographic conjecture

$$J(A, B, C)|_{|\Omega\rangle} = 0 \quad (\text{E2})$$

for the CFT vacuum $|\Omega\rangle$. Note that this holds for any CFT, even the chiral ones. This fact can be independently verified by the operator-based method as follows. Suppose the boundary circle has a circumference of L and $0 < x_1 < x_2 < x_3 < x_4 < L$. We can derive Eq. (E2) using the Cardy-Tonni expression Eq. (B18) [16]. Let $B_1 = [x_1, x_2]$ and $B_2 = [x_3, x_4]$ with $0 \leq x_1 < x_2 < x_3 < x_4 < L$, and $A = [x_2, x_3]$ and $C = [x_4, L + x_1]$, then

$$K_{AB} = \frac{L}{\pi} \int_{x_1}^{x_4} dx \frac{\sin(\pi(x - x_1)/L) \sin(\pi(x_4 - x)/L)}{\sin(\pi x_{14}/L)} (T(x) + \bar{T}(x)) \quad (\text{E3})$$

and

$$K_{BC} = \frac{L}{\pi} \int_{x_3}^{L+x_2} dx \frac{\sin(\pi(x - x_3)/L) \sin(\pi(L + x_2 - x)/L)}{\sin(\pi(L - x_{23})/L)} (T(x) + \bar{T}(x)) \quad (\text{E4})$$

Computing the commutator using Eq. (B21) and identifying $T(x)$ with $T(x+L)$ for $x \in [x_1, x_2]$ we find $J(A, B, C)$ identically vanishes.

Now we discuss a case with a pair of crossing angles $\{\theta_1, \theta_2\}$. This is similar to the setup discussed above, except now we have a BTZ black hole; see Fig. 14(b) and (c). We shall derive an expression for the modular commutator using our proposed correspondence; this result shall be compared against a numerical experiment, discussed in Section E1.

Let us first derive the expressions for the crossing angles on the AdS side. Using the results in Section D2, for any black hole mass, one can verify

$$\cos \theta_1 = 2 \frac{X_{13} X_{45}}{X_{14} X_{35}} - 1 \quad \text{and} \quad \cos \theta_2 = 2 \frac{X_{01} X_{24}}{X_{02} X_{14}} - 1, \quad (\text{E5})$$

where the fractions $(X_{13} X_{45})/(X_{14} X_{35})$ and $(X_{01} X_{24})/(X_{02} X_{14})$ can be interpreted as the effective cross ratios; see Eq. (D16) for a comparison. The coordinates $\{X_i\}_{i=0}^5$ are the endpoints on the X axis, and they are related to the coordinates on the boundary circle $\{x_j\}_{j=1}^4$ according to the relation $X_j = \exp(2\pi\sqrt{M}x_j/L)$ for $j = 1, 2, 3, 4$, $X_0 = \exp(-2\pi\sqrt{M})X_3$ and $X_5 = \exp(2\pi\sqrt{M})X_2$. In other words, $\cos \theta_1$ and $\cos \theta_2$ are functions of the boundary coordinates $\{x_j\}_{j=1}^4$ and \sqrt{M}/L .

Now we relate the crossing angles to the CFT data. When the mass of the BTZ black hole satisfies $M \gg 1$, the boundary is dual to a CFT thermal state ρ^β at high temperature ($\beta \ll L$ since $\sqrt{M} = L/\beta$). In this regime, our proposal reads:

$$J(A, B, C)_{\rho^\beta} = \frac{\pi c_-}{6} (\cos \theta_1 - \cos \theta_2). \quad (\text{E6})$$

A minus sign appears in the second term due to the rule we specified above. (Note that we only expect Eq. (E6) to hold for $\beta \ll L$ even for holographic CFTs, as this is the range of temperature in which a semiclassical BTZ black hole exists in a quantum theory. The temperature in this range is well above the Hawking-Page transition temperature [34–36].) The two angles are related to the effective cross-ratio

$$\eta_{\text{eff}}^\beta(a, b, c) \equiv \frac{\sinh(\pi a/\beta) \sinh(\pi c/\beta)}{\sinh(\pi(a+b)/\beta) \sinh(\pi(b+c)/\beta)} \quad (\text{E7})$$

according to

$$\begin{aligned} \cos \theta_1 &= 2\eta_{\text{eff}}^\beta(|AB_1|, |B_2|, |B_1C|) - 1, \\ \cos \theta_2 &= 2\eta_{\text{eff}}^\beta(|B_2C|, |B_1|, |AB_2|) - 1, \end{aligned} \quad (\text{E8})$$

where $|A|$ is the length of the boundary interval A . As a simple consequence, Eq. (E7) gives nonzero result only if $x_{12} \neq x_{34}$, that is $|B_1| \neq |B_2|$.

1. Numerical test of Eq. (E6)

Eq. (E6) can be tested numerically for chiral thermal states of a free fermion CFT, which is a nonchiral 1+1D CFT with central charge $c = 1/2$ ($c = c_L = c_R$). Numerical techniques are discussed in Section F. Consider a chiral thermal state $\rho^{(\beta_L, \beta_R; L)}$, i.e., a chiral thermal state with inverse temperature β_L (β_R) for the left (right) moving modes on a circle with length L . Consider the chiral thermal state with $\beta_R \rightarrow +\infty$ and consider the ABC partition in Fig. 14. It follows directly from the discussion in the previous Section that

$$J(A, B, C)_{\rho^{(\beta_L, +\infty; L)}} = \frac{\pi}{6} \left(\frac{\sinh(\pi|AB_1|/\beta) \sinh(\pi|B_1C|/\beta) - \sinh(\pi|AB_2|/\beta) \sinh(\pi|B_2C|/\beta)}{\sinh(\pi|AB|/\beta) \sinh(\pi|BC|/\beta)} \right). \quad (\text{E9})$$

First, a consequence of Eq. (E9) is that $J(A, B, C)_{\rho^{(\beta_L, +\infty; L)}} = 0$ when $x_{12} = x_{34}$ (i.e., $|B_1| = |B_2|$). We can therefore make slight perturbation around this ‘‘symmetric’’ configuration and see how J changes.

Eq. (E9) is confirmed numerically for $\beta_L \ll L$ in the chiral thermal state of the free fermion CFT; see Fig. 15(a). We see from this figure that when β_L/L is small ($\beta_L/L < 0.2$) the prediction fits the data well.

Second, if we keep $\beta_L = 0.15L$ and vary the sizes of the intervals, our conjecture agrees with the data in good precision. This is illustrated in Fig. 15(b). We note however that if the size of $|A|$ or $|C|$ are small compared with β_L , the data can deviate from our formula. The correction may come from two sources. (1) The free Majorana fermion

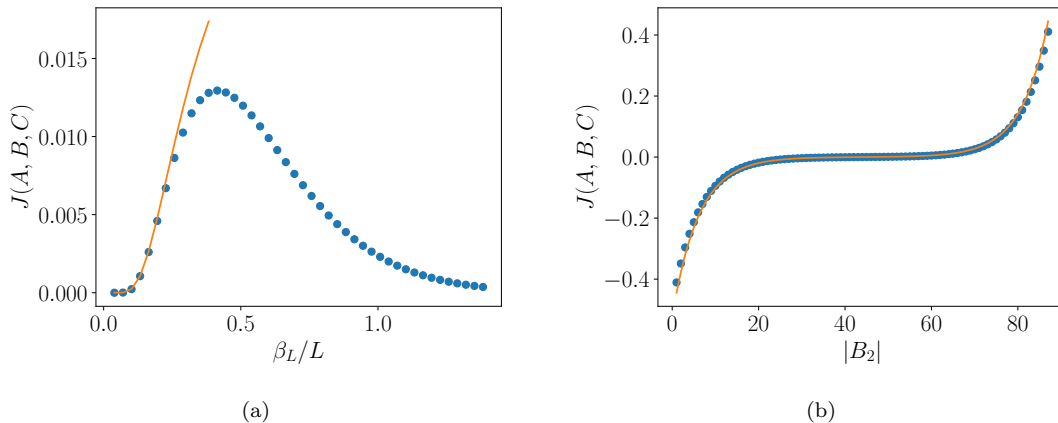


FIG. 15. Modular commutator $J(A, B, C)$ of a chiral thermal state $\rho^{(\beta_L, \beta_R, L)}$ of the free Majorana fermion CFT, where B is composed of disjoint intervals B_1 and B_2 . We fix $\beta_R = \infty$ and $L = 128$ throughout the simulation. Blue dots represent numerical data and the orange line represents fitting from Eq. (E9). (a) We fix the lengths of intervals $|A| = |C| = L/4$, $|B_1| = L/4 - 2$, $|B_2| = L/4 + 2$, and varying β_L . (b) We fix $\beta_L = 0.15L$ and $|A| = |C| = 20$ and vary $|B_2|$.

CFT has $c = 1/2$ and it is not a holographic CFT, which is defined in the large central charge limit. (2) Even for holographic CFT, the bulk area operator and the boundary modular Hamiltonian differ by subdominant terms (that is, modular Hamiltonian of the bulk gravity). These contributions might become important when $|A|, |C| < \beta_L$ and the interval AB or BC cover most of the circle. We leave the study of these corrections for future work.

Appendix F: Free fermion numerical methods and simulation results

We discuss the numerical method we use for the simulation of free fermion systems. The main simplification arising in this setup is that both the ground states and thermal states are Gaussian. Therefore, the state is determined by the correlation matrix [37].

1. Free fermion simulation of the Chern insulator

Consider first the $U(1)$ symmetric case with a chain of fermionic degrees of freedom. The creation and annihilation operators are denoted c_i^\dagger, c_i , where $i = 1, 2, \dots, N$ and $\{c_i^\dagger, c_j\} = \delta_{ij}$. A Gaussian state ρ is completely determined by the $N \times N$ correlation matrix

$$C_{ij} = \text{Tr}(\rho c_i^\dagger c_j) \quad (\text{F1})$$

The modular Hamiltonian $K = -\ln \rho$ is of the fermionic bilinear form

$$K = \sum_{ij} K_{ij} c_i^\dagger c_j. \quad (\text{F2})$$

The matrix K is related to the correlation matrix by

$$K = \ln \frac{I - C}{C}. \quad (\text{F3})$$

The formula is applicable to any subsystem. Let C_{AB} be the submatrix restricted to the fermions in region AB , then

$$K_{AB} = \ln \frac{I - C_{AB}}{C_{AB}}. \quad (\text{F4})$$

The modular commutator can then be computed by

$$J(A, B, C) = i \text{Tr}(C_{ABC}[K_{AB}, K_{BC}]) \quad (\text{F5})$$

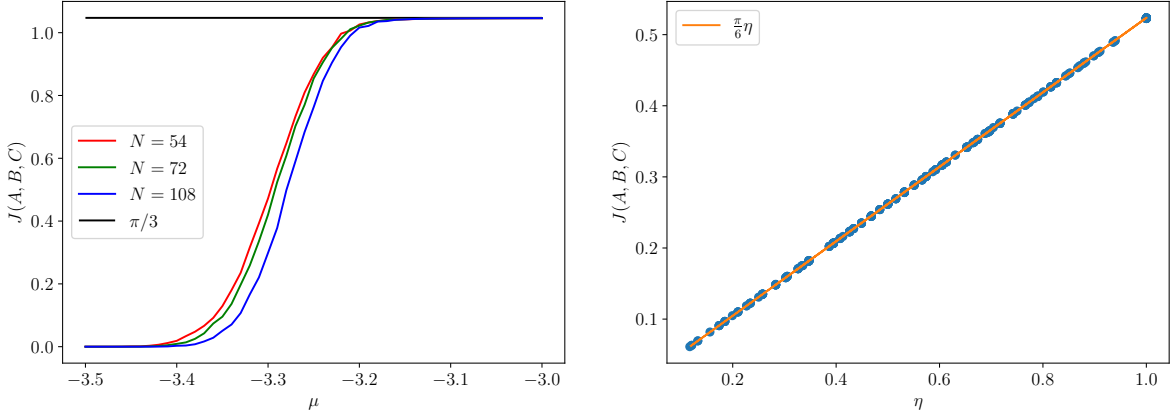


FIG. 16. Left: Modular commutator $J(A, B, C)$ versus chemical potential μ in the disordered Chern insulator. We choose $B = 2\pi/9$ and the width of the strips to be $w = 6$, and A, B, C cover the entire circle. Disordered average is performed on 300 samples. Right: Modular commutator $J(A, B, C)$ versus η in $p + ip$ topological superconductor.

The Chern insulator can be modeled by the Hofstadter model [38–40] in a two-dimensional square lattice,

$$H = -t \sum_{\vec{x}, \vec{a}} (c_{\vec{x}}^{\dagger} e^{-i\vec{a} \cdot \vec{A}(\vec{x})} c_{\vec{x}+\vec{a}} + h.c.) + \mu \sum_{\vec{x}} c_{\vec{x}}^{\dagger} c_{\vec{x}} \quad (\text{F6})$$

where \vec{a} runs over lattice vectors and \vec{A} is the vector potential which equals $\vec{A} = (0, Bx_1)$ for the square lattice in the Landau gauge and B is the flux per unit cell. We choose $\mu/t = -2.0$ and $B = \pi/2$ such that the lowest band is filled. The band has Chern number 1, which gives the chiral central charge $c_- = 1$. We put the system on an open cylinder with horizontal direction compactified on a circle with circumference N and height M . We compute the modular commutator $J(A, B, C)$, where A, B, C are rectangular strips on the boundary with the horizontal length L_A, L_B, L_C and the same width w , where all of $L_A, L_B, L_C, w, M - w$ are sufficiently large compared to the correlation length.

The chiral edge mode is robust against small disorder. One may add an Anderson term [41],

$$H = -t \sum_{\vec{x}, \vec{a}} (c_{\vec{x}}^{\dagger} e^{-i\vec{a} \cdot \vec{A}(\vec{x})} c_{\vec{x}+\vec{a}} + h.c.) - \mu \sum_{\vec{x}} c_{\vec{x}}^{\dagger} c_{\vec{x}} + \sum_{\vec{x}} V_{\vec{x}} c_{\vec{x}}^{\dagger} c_{\vec{x}}, \quad (\text{F7})$$

where $V_{\vec{x}}$'s are independent random variables drawn from the uniform distribution in $[-W/2, W/2]$, and W is the disorder strength. The original Landau band gets broadened into a disordered band with width $O(W)$ that consists of localized eigenstates on the edge of the band and extended states in the middle of the band. As the chemical potential gets varied, the system goes through an Anderson localization transition and the Hall conductance jumps from 0 to 1 (in the unit of e^2/h). It is believed that the Anderson localization transition is responsible for the plateau of Hall conductance observed in experiments [42], although the nature of the transition is still under debate [43, 44].

Since the modular commutator detects the chiral central charge, we expect there to be a similar transition in the modular commutator. Let A, B, C be equal-size strips that cover the whole boundary, which gives $J(A, B, C) = \pi c/3$, it is expected then that the disordered averaged J has a plateau transition as one varies the chemical potential. This is indeed observed, see Fig. 16. This also provides numerical evidence of the claim that J is robust against disorder, as argued using entanglement bootstrap in the main text.

2. Free fermion simulation of the $p + ip$ topological superconductor

In this Section we consider the real fermions (Majorana fermions) with \mathbb{Z}_2 fermionic parity symmetry. Let ψ_i , $i = 1, 2, \dots, 2N$ be the Majorana operators with anticommutation relations $\{\psi_i, \psi_j\} = 2\delta_{ij}$, a Gaussian state ρ is completely specified by the correlation matrix, which is a real skew-symmetric $2N \times 2N$ matrix

$$M_{ij} = \text{Tr}(-i(\psi_i \psi_j - \delta_{ij}) \rho). \quad (\text{F8})$$

It can be block diagonalized by an orthogonal matrix $O \in O(2N)$,

$$M = O(\text{diag}(n_i) \otimes (i\sigma^y))O^T, \quad (\text{F9})$$

where σ^y is the Pauli operator, and $n_i \in [-1, 1]$. Similar to the complex fermion case one can write the modular Hamiltonian as

$$K = \frac{i}{2} \sum_{ij} K_{ij} \psi_i \psi_j, \quad (\text{F10})$$

where K_{ij} is a real skew-symmetric matrix

$$K = O \left(\text{diag} \left(\frac{1}{2} \ln \frac{1-n_i}{1+n_i} \right) \otimes (i\sigma^y) \right) O^T, \quad (\text{F11})$$

One may obtain the modular Hamiltonian of any subsystem by block diagonalizing submatrices of M . The modular commutator can be computed by

$$J(A, B, C) = \text{Tr}([K_{AB}, K_{BC}]M_{ABC}). \quad (\text{F12})$$

As a concrete application, we consider the BdG p -wave superconductor Hamiltonian [45]

$$H = \sum_{m,n} -t(c_{m+1,n}^\dagger c_{m,n} + c_{m,n+1}^\dagger c_{m,n} + h.c.) - (\mu - 4t)c_{m,n}^\dagger c_{m,n} \quad (\text{F13})$$

$$+ (\Delta c_{m+1,n}^\dagger c_{m,n}^\dagger + \Delta^* c_{m,n} c_{m+1,n}) + (i\Delta c_{m,n+1}^\dagger c_{m,n}^\dagger - i\Delta^* c_{m,n} c_{m,n+1}) \quad (\text{F14})$$

of $L_x L_y$ complex fermions. This can be recast into a Majorana fermion Hamiltonian with $2L_x L_y$ Majorana fermions using

$$\psi_{m,n,1} = c_{m,n}^\dagger + c_{m,n}, \quad \psi_{m,n,2} = i(c_{m,n}^\dagger - c_{m,n}). \quad (\text{F15})$$

We take the boundary condition in the x direction to be Neveu-Schwarz (NS), and y direction to be open. In this setting there is no Majorana zero mode and the ground state is unique. We choose $t = 1$, $\Delta = 0.5$ and $\mu = 1$ such that the system is in the topologically nontrivial phase. On the boundary there is a chiral Majorana fermion CFT in the NS sector, with $c = 1/2$. In the actual finite-size simulations we choose $L_x = 36$ and $L_y = 20$ and the width of strips A, B, C to be $w = 8$; these strips are placed near the lower boundary and we varied the horizontal lengths of the strips. We find perfect agreement with the analytical result $J(A, B, C) = \pi c \eta / 3$, see Fig. 16.

3. Chiral thermal state on the lattice

We can also construct a chiral thermal states for free fermion systems directly on a 1+1D lattice without going to 2+1D. Consider a one-dimensional complex fermion chain in infinite space with Hamiltonian

$$H = -t \sum_i (c_i^\dagger c_{i+1} + h.c.) \quad (\text{F16})$$

The Hamiltonian can be diagonalized using Fourier modes $c(k) = \sum_j c_j e^{-ikj}$,

$$H = \int_{-\pi}^{\pi} dk \epsilon(k) c^\dagger(k) c(k), \quad (\text{F17})$$

where

$$\epsilon(k) = -2t \cos k. \quad (\text{F18})$$

The momenta near the Fermi points $k = \pm\pi/2$ determine the low-energy CFT, which is a 1+1D free Dirac fermion. We will choose $t = 1/2$ to normalize the Hamiltonian such that the speed of light is one. A quantum state is completely specified by the expectation value of $n(k) = c^\dagger(k)c(k)$, where for the ground state we have $n(k) = \Theta(-\epsilon(k))$ and

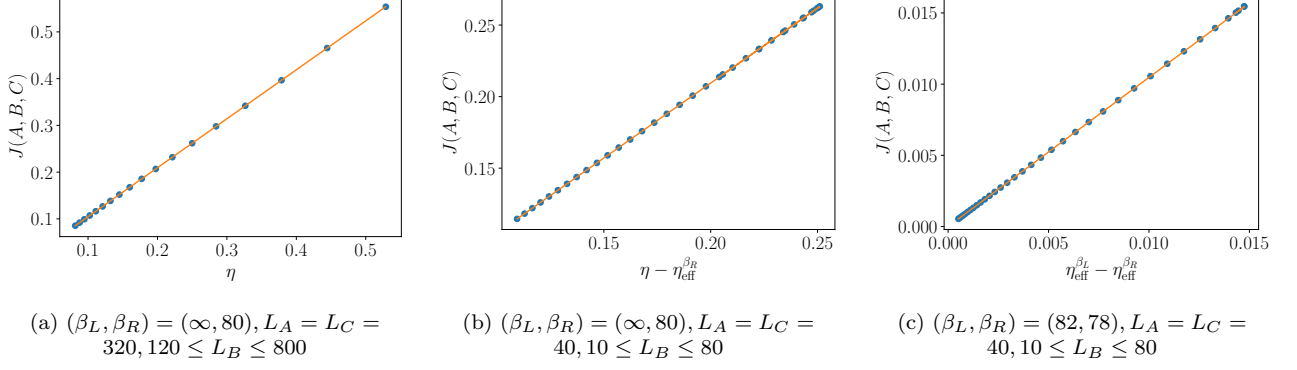


FIG. 17. Modular commutators in chiral thermal state of free fermion CFT on an infinite line.

$\Theta(x)$ is the step function. For a chiral thermal state with inverse temperatures (β_L, β_R) , we expect two Fermi-Dirac distributions depending on the chirality,

$$n(k) = \begin{cases} 1/(1 + e^{\beta_L \epsilon(k)}) & \text{if } k < 0, \\ 1/(1 + e^{\beta_R \epsilon(k)}) & \text{if } k > 0 \end{cases} \quad (\text{F19})$$

This completely determines the state. In particular, we can write down the correlation matrix

$$C_{mn} = \frac{1}{2\pi} \int_{-\pi}^{\pi} dk n(k) e^{ik(n-m)}, \quad (\text{F20})$$

from which we compute the modular commutators. We note that this construction only works well if $\beta_L, \beta_R \gg t^{-1}$. This is because the system is no longer described by a CFT at high energies. At finite sizes the same construction also works but one needs to substitute the integrals in k by a finite sum over discrete momenta. The CFT computation in the main text implies the modular commutator

$$J(A, B, C) = \frac{\pi}{3} (\eta_{\text{eff}}^{\beta_L}(L_A, L_B, L_C) - \eta_{\text{eff}}^{\beta_R}(L_A, L_B, L_C)), \quad (\text{F21})$$

where $\eta_{\text{eff}}^{\beta}$ is defined in Eq. (E7). As $\beta \rightarrow \infty$, $\eta_{\text{eff}}^{\beta} \rightarrow (x_{12}x_{34})/(x_{13}x_{24}) = \eta$. In the limit in which all the intervals are significantly larger than β , $\eta_{\text{eff}}^{\beta} \rightarrow 0$. Below we study two examples, both with $t = 1/2$. (1) $(\beta_L, \beta_R) = (\infty, 80)$, and (2) $(\beta_L, \beta_R) = (82, 78)$. The first example is relevant to the edge of chiral topological order, and the second example is close to the time reversal invariant case so we can expect J to be small. In the first case we also study two ranges of the subsystem sizes which are much larger or comparable to β_R . If all sizes are large compared to β_R then we get $J = \pi c \eta / 3$, like on the edge of chiral topological order. Our numerical result perfectly agrees with the predictions.